Broadcast Control for Anti-drone Systems

Yasuo Fujishima

Department of Mechanical Systems Engineering
Graduate School of Engineering, Nagoya University

2024

Contents

List of Figures

List of Tables

List of Symbols

$\mathbb{R}$	:	Set of real numbers
$\mathbb{R}_{0+}$	:	Set of zero or positive real numbers
$\mathbb{R}_{+}$	:	Set of positive real numbers
$\mathbb{N}$	:	Set of natural numbers
$t \in \mathbb{R}_{0+}$	:	Continuous time
$k \in \mathbb{N}$	:	Discrete time index
$\tau \in \mathbb{R}_{0+}$	:	Sampling period
I_N	:	$N \times N$ identity matrix
$0_{M \times N}$	:	$M \times N$ zero matrix

Chapter 1

Dissertation Introduction

Recently, autonomous aerial vehicles (so-called drones) are widely used. The International Civil Aviation Organization (ICAO) formulated the guidelines for safe drone operation [1], whereas there have been incidents such that a drone, which may be hobby-use, intrudes into an off-limits area such as an airport and a power plant, and causes serious accidents [2, 3].

To address the problem, we propose a new surveillance system against the drone in this dissertation. We call such a surveillance system an "anti-drone system". Figure 1.1 illustrates an example of the anti-drone system. In the figure, the system has sensors such as radar or cameras on the base station for detecting illegal drones in the detectable area. If the drone shape in the image data acquired by the camera is large, the drone may be detected with high probability. Such ease of drone detection is called detection probability. Since the drone is small and movable, and difficult to be detected by the fixed sensors, it is important to increase detection probability by the anti-drone system. However, the sensors are often stationary on the ground or in the building as in Figure. 1.1. Therefore, the anti-drone system can not detect the drone when the drone escapes into the area that the sensor does not cover.

This dissertation thus proposes a new radar surveillance system to expand the area of detection and improve the detection probability of intruders.

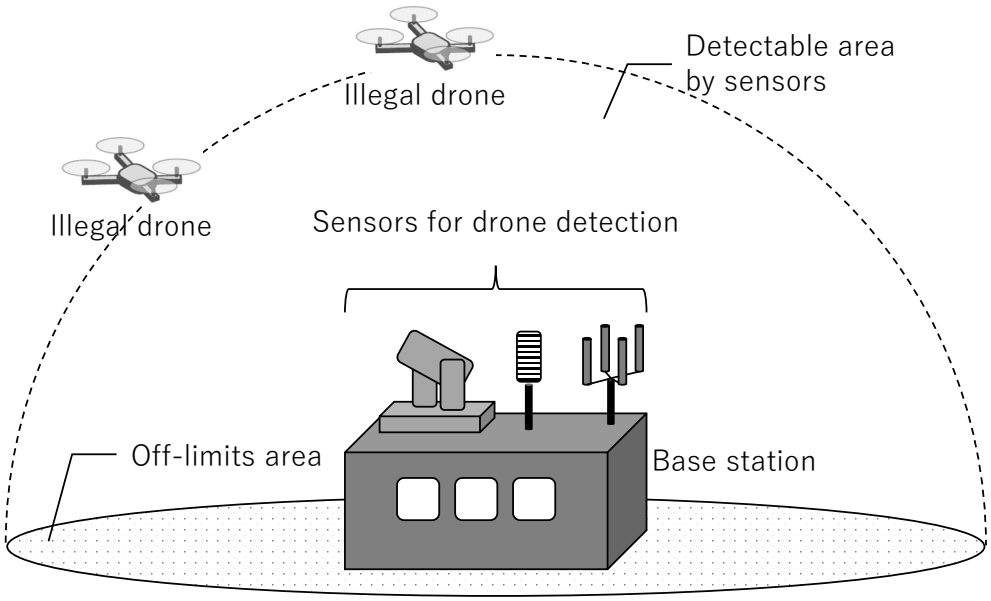

Figure 1.1: Anti-drone system.

1.1 Illegal Drone Incidents

Figure 1.2 in [3] depicts the number of drone incidents occurred around the airport and we see that the number is increasing. Note that the decrease in 2020 is due to COVID-19.

About each incident in the world, the website [2] shows with updating. The sample is illustrated in Figure 1.1. One of the famous and serious incidents is the case that occurred at Gatwick Airport, which affected more than 1,000 flights and about 140,000 passengers [4].

Thus, various types of anti-drone systems are proposed and the part of them are in practice.

1.2 Conventional Anti-drone Systems

Anti-drone systems to detect unexpected drones (which are called here the intruders) are becoming more and more important. Thus, various studies have been conducted

Table 1.1: Drone incidents examples [2].

Incident	Target	Location	Date
Tourist flying drone near Dalada Maligawa arrested	Law Enforcement / First Responders	Kandy, Sri-Lanka	July 11, 2023
Drone used to fly items into Stockton's Holme House prison	Prisons	Stockton-on-Tees, England, United Kingdom	July 10, 2023
Drone loaded with drugs crashes in Lahore's Kahna	Government / Military	Kahna, Lahore, Pakistan	July 7, 2023
Drone Falls and Crashes Into Disney Park Building	Entertainment / Media	Paris, France	July 4, 2023
Drone Spotted Over Prime Minister Modi's Residence	Government / Military	New Delhi, India	July 3, 2023
Ten drones caught on unauthorized flights above Song Festival	Stadiums	Riga, Latvia	July 2, 2023

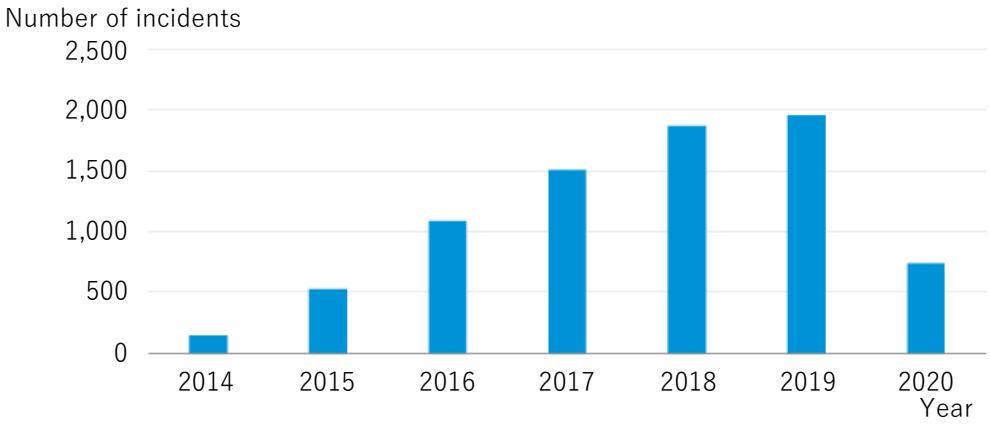

Figure 1.2: Number of drone incidents around airport [3].

on anti-drone systems. For example, several anti-drone systems have been surveyed in [5, 6]. Figure 1.3 illustrates a detection method classification presented in [6]. As illustrated in the figure, the existing systems are classified by the sensor type, detection range, and challenges. The survey can be summarized as Table 1.2. For example, camera-based anti-drone systems have been proposed in [7–14]. However, the systems have the drawback that the detection accuracy is affected by sunlight, by which it cannot be used during the hours of darkness. On the other hand, a microphone-based system has been developed in [15–19], while the range of detection is relatively smaller compared with the other types of sensors and the resolution will be low around a noise source. Moreover, Radio Frequency (RF) based anti-drone systems, which detect radio waves emitted from an intruder at communicating with the operator and check the radio wave patterns from the pre-arranged database, have been proposed in [20–25]; however, they need a database of the relation between the intruders and radio waves and cannot be used for intruders that do not emit radio waves.

Meanwhile, radar-based anti-drone systems are known to be promising for overcoming the above drawbacks. Radars are not affected by sunlight and the range of detection is relatively larger. In addition, they can detect intruders which do not emit radio waves. On the other hand, there are technical issues to be solved for realizing

radar-based anti-drone systems. In particular, for small-size drones, the radar cross section (RCS; received signal level of the radar echo for the transmitted angle) is low, which makes the detection difficult. It has been experimentally shown that the range of detection is less than 250m [26–29], though the potential range of radar-based systems is 3000m [5]. This motivates us to develop a radar-based surveillance system with a larger range of detection. Additionally, the anti-drone systems using the bistatic radar for drone detection have been also proposed and field experiments with the actual drone have been carried out [30–33]. In the previous experiments, it has been indicated that the small drone can be detected by the bistatic radar system. However both the transmission and receiving antennas are placed in the fixed location in these conventional systems, which will result in intruder loss.

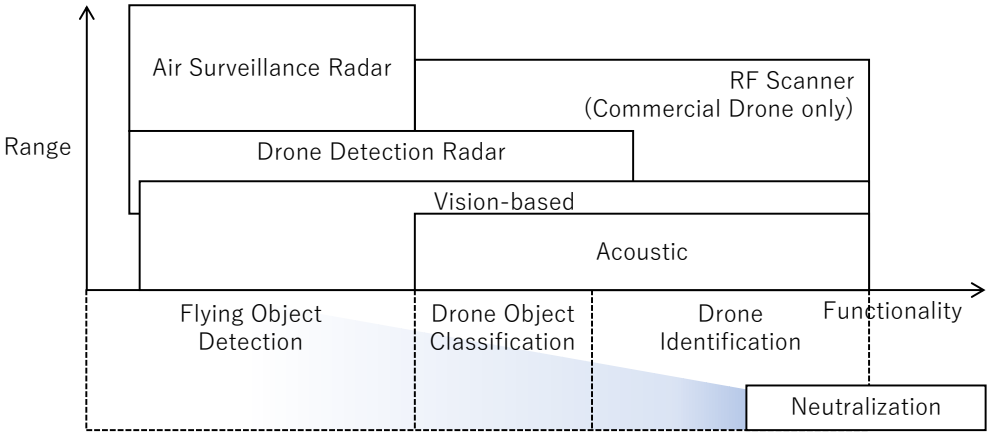

Figure 1.3: Detection method classification depicted in [6].

Next, we show an example for each sensor.

Figure 1.4 illustrates a sample of the detection result by the image processing based on the deep learning technique proposed in [13]. In the figure, the actual number of drones is one and the other objects are birds. The figure indicates that the drone is correctly detected by the camera-based approach even if the non-target such as bird is also captured in the same image. However, the camera-based detection system can not work in the evening. Additionally, we can find that the field of view of the camera

Table 1.2: Researches on anti-drone systems for detecting intruders.

Detection Devise	Results	Drawbacks
Camera	[7–14]	The operation time is limited.
Microphone	[15–19]	The range of detection is small, and the resolution is low around a noise source.
RF Sensor	[20–25]	A database is needed and it cannot be used for intruders that do not emit radio waves.
Radar	[26–33]	A method to enhance the signal level is needed.

is commonly narrow from the figure.

Figure 1.4: Example of camera-based detection result proposed in [13].

Figure 1.5 depicts an example of the acoustic-based detection method, which is proposed in [17]. From the figure, we can confirm that various methods of signal processing under the assumption of the capability of acoustic signals received with the microphones. Thus, these signal processing methods can not work when the level of the received signal is low due to the long-distance or drone's silent flight.

Figure 1.6 illustrates an example of RF-based detection processing in [22]. The RF signal is input into the deep neural network called VGG19, the features are extracted, and the features are classified by the Support Vector Machine. Thus, we see that the database is needed for classifying the types of drones.

Figure 1.7 depicts an example of the conventional radar anti-drone systems proposed in [30]. The target has unique reflection characteristics corresponding to the shape and the level of the reflected signal from the target is not necessarily maximum for the angle of the transmitter. Therefore, the transmission and receiving antenna is separated from each other in [30].

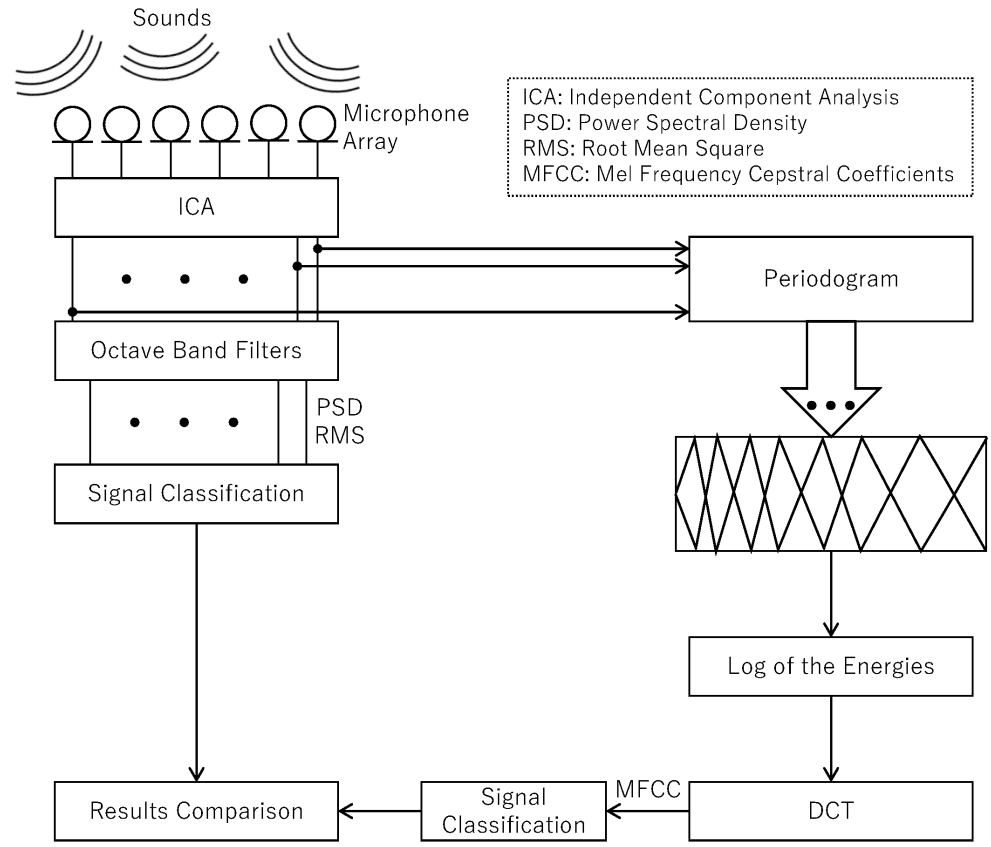

Figure 1.5: Example of acoustic-based detection method proposed in [17].

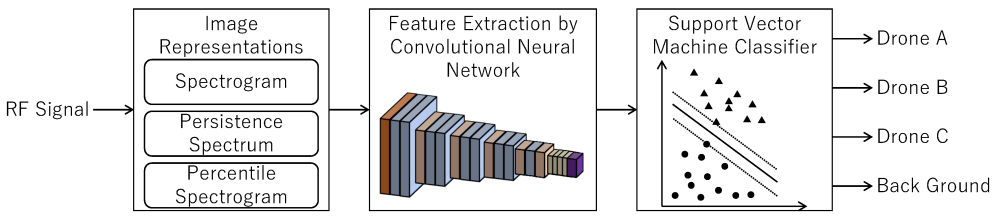

Figure 1.6: Example of RF-based detection method proposed in [22].

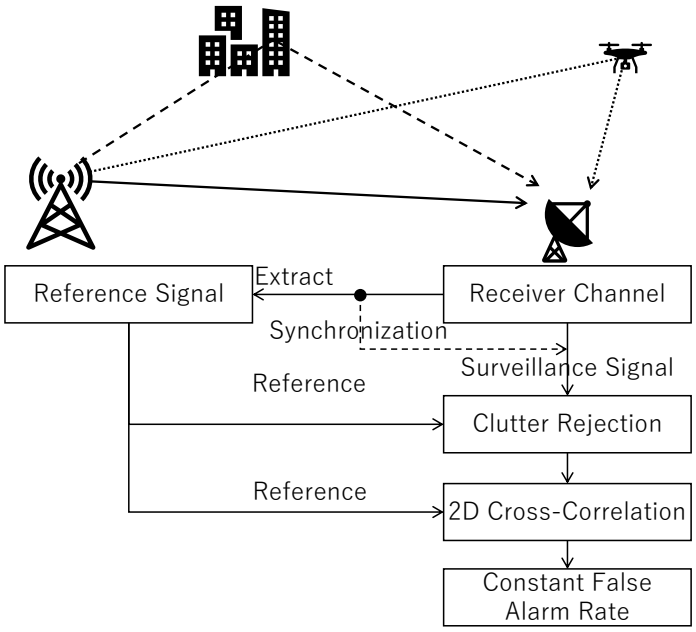

Figure 1.7: Example of radar-based detection method proposed in [30].

On the other hand, the Japanese government has also considered the concept of the anti-drone system. Recently, the anti-drone systems which realize the concept [34–42] become practical due to increasing drone incidents.

1.3 Control of Multi-vehicle Systems

From the previous section, we can find that the detection in the anti-drone system is mainly realized by the stationary sensors in the ground or the building. Thus, target loss may occur when the acquired data by the sensors is affected by the noise or occlusion [14] and the unexpected drone detection system using the mobile sensors is needed such as presented in [43]. This is the motivation of our research. Since some drones will try to intrude into the restricted area simultaneously, we consider the multiple mobile sensors (i.e., the sensors mounted in the vehicles). Therefore, the cooperative control technique is also needed in the anti-drone system considered in this dissertation and we show the conventional cooperative control in the following

section.

The research about cooperative control for multi-vehicle systems has been conducted [44–49]. In most research, the vehicles are assumed to be able to acquire the relative positions [45], distances [46, 47], or angles [46–48] by wireless communication or measurement. Additionally, the received signal levels of radio waves are utilized for the formation control instead of the relative distance. These researches are classified into three categories illustrated in Figure 1.8 and Table 1.3. Figure 1.8a, 1.8b, and 1.8c depict the centralized control, distributed control with the leader, and distributed control without the leader, respectively. Each characteristic is summarized in Table 1.3.

In the centralized control (Figure 1.8a), the leader computes important information such as the control inputs or target positions of the other vehicles, and sends them to them. Thus, the leader communicates with the other vehicles individually, otherwise, it must send the same information for all vehicles, whose amount increases in proportion to the number of vehicles.

On the other hand, the vehicles of distributed control systems illustrated in Figure 1.8b and 1.8c send information only to the neighbors which means that the vehicles are within communication distance. However, the systems need a complex wireless communication architecture. Especially, their vehicles should communicate by full-duplex to unspecified ones whose number changes during the communication period.

We show the examples of each system illustrated in Figure 1.8 as follows.

1.3.1 An Example of Centralized Control

Figure 1.9 illustrates an example of the centralized control system proposed in [46, 47]. In the system, the leader and the follower are called “parent” and “child”, respectively. The parent mounts high-performance sensors and can measure relatively correct information about the states compared with the child. Thus, the parent can arrive at the target position independently, whereas the child will be lost in the single navigation. Under these assumptions, [46, 47] propose a system in which the parent

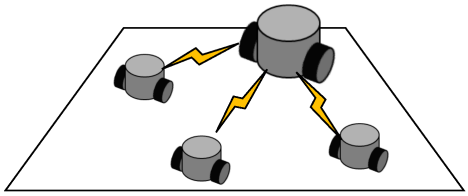

(a) Centralized control system.

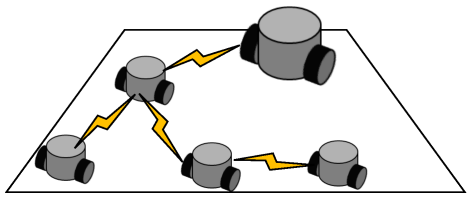

(b) Distributed control system with leader.

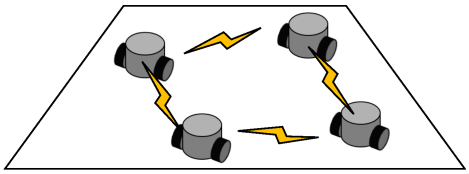

(c) Distributed control system without leader.

Figure 1.8: Communication system of cooperative control.

Table 1.3: Comparison between centralized and distributed cooperative control.

Communication system	Abstract	Drawbacks
Centralized control	The leader or base station sends information to each vehicle.	There is no scalability in communication resources.
Distributed control with the leader	The leader sends information only to the vehicles which can communicate with the leader.	The communication or measurement system for acquiring the states of the neighbors becomes to be complex.
Distributed control without the leader	The vehicles send information to each other or measure states of the neighbors.	The communication or measurement system for acquiring the states of the neighbors becomes to be complex.

guides the children to the target area. The concept is realized as follows. First, the parent transmits the signal including self-state to all children and each child replies to the parent at once. Then, the parent estimates the relative distances and angles between itself and the children. Finally, the parent broadcasts the distances and angles to them. Therefore, the number of communications and the information amount also increase as the number of vehicles increases.

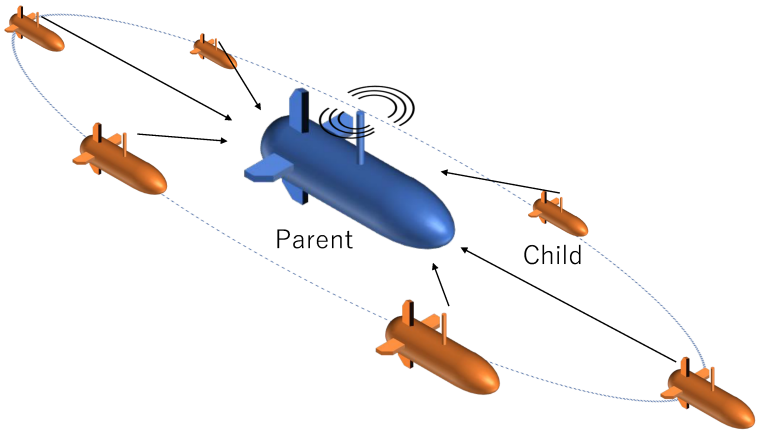

Figure 1.9: Example of centralized control systems proposed in [46, 47].

1.3.2 An Example of Distributed Control with Leader

Figure 1.10 illustrates an example of the distributed cooperative control systems composed of the single leader and multi-follower [45]. [45] proposes the cooperative followers' algorithm for tracking the leader with the same yaw angles as it and 1.10b depicts the simulation result. In such a system, all the followers are required to be able to communicate with the leader directly or by relaying the other followers. The network structure like Figure 1.10a is allowed to change, which indicates the vehicle communicates with the unspecified ones. This seems to cause the complexity and uncertainty of the multi-vehicle system. Additionally, the followers' target positions are calculated in the leader and the computational complexity increases in proportion to the number of followers.

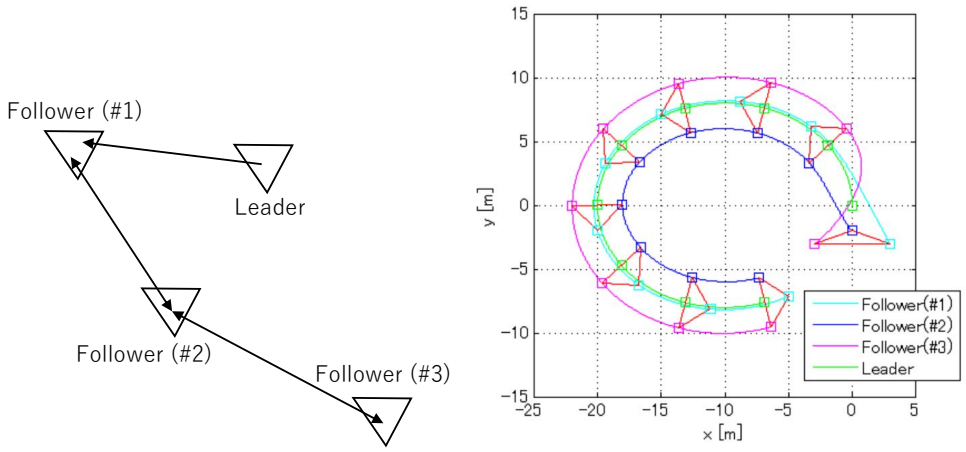

(a) Network structure example.

(b) Simulation result.

Figure 1.10: Example of distributed control systems with leader illustrated in [45].

1.3.3 An Example of Distributed Control Without Leader

Figure 1.11 illustrates an example of the distributed control systems without the leader [50]. Figure 1.11a and Figure 1.11b show a network structure and the simulation result of obstacle avoidance. [50] proposes the distributed Model Predictive Control (MPC). The proposed method is derived from the centralized version as follows. First, the optimization problem for the centralized MPC is defined. Next, the problem is separated into some small problems. Each vehicle solves such a small problem at the control period and shares information with the neighbor vehicles corresponding to the network structure as Figure 1.11a. In the processing, the leader is not needed and the distributed system without the leader is realized. However, the system has the same challenges as one explained in Section 1.3.2 about network complexity.

1.3.4 Cooperative Vehicle Control for Anti-drone Systems

The anti-drone system should work on all days and the radar device is needed as mentioned in Section 1.2. But the drone has unique reflection characteristics for the transmitted signal from the radar so-called RCS [51–53]. Figure 1.12 depicts an example of the drone (left) and the RCS (right) [51]. Therefore, the radar mounted on

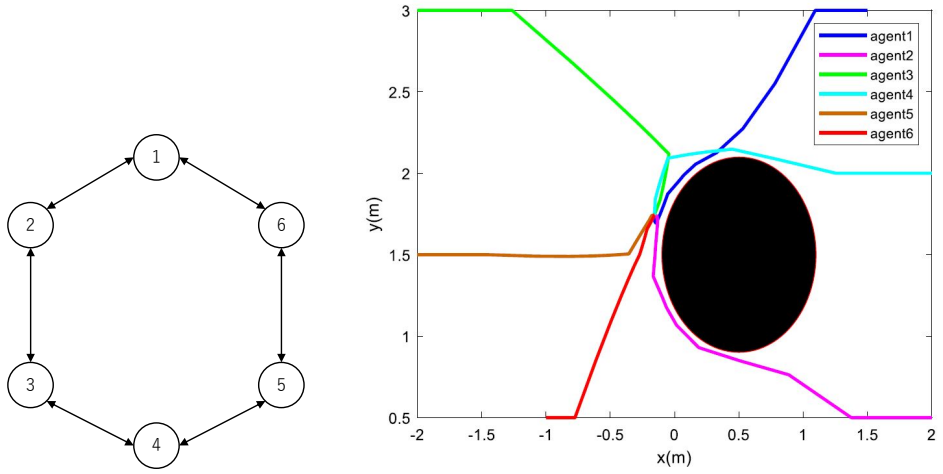

(a) Network structure example. **(b)** Simulation result.

Figure 1.11: Example of distributed control systems without leader presented in [50].

the ground or the building may not be able to detect the unexpected drone due to the weak level of the received signal on the radar. Although the high-performance radar can detect the drone even if the received signal level is weak, it becomes expensive.

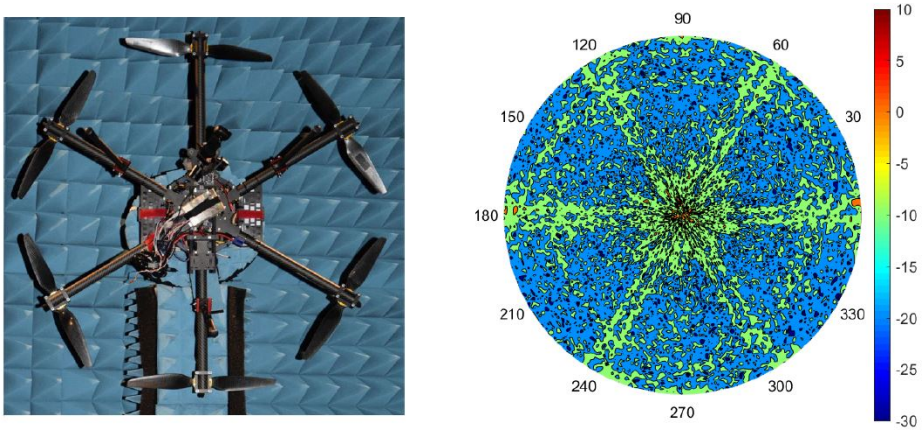

Figure 1.12: Example of drone RCS shown in [51].

On the other hand, the signal level received by the radar is strengthened by moving the vehicles. By introducing multi-vehicle, the anti-drone system can detect multi-drone. However, the positions of the target drones are unknown to the system and

the reference formation of the vehicles can not be explicitly set. Additionally, the communication systems illustrated in Section 1.3.1, 1.3.2, and 1.3.3 are complex and also become expensive.

1.4 Broadcast Control

The alternative control algorithm of the multi-vehicle system called as the broadcast control is also proposed [55, 56]. In the broadcast control, a simple communication system is assumed as compared to the other conventional algorithms in Section 1.3. Concretely, the common scalar signal is only transmitted from the base station to all vehicles and the opposite communication from the vehicle to the base station is not operated.

Figure 1.13 illustrates the communication of the broadcast control. The scalar signal depends on the output of the objective function for evaluating the vehicles formation and the optimization for the objective function is achieved under some assumptions.

The broadcast control algorithm does not need information about the system of the dynamics in operation. Thus, the algorithm may be effective for the system with the unknown components such as the RCS and we focus on the algorithm.

However, the broadcast control for the anti-drone system such as radar surveillance was not established. Additionally, it was assumed that the vehicle dynamics was single-integrator system. These are challenges about the broadcast control algorithm.

1.5 Contributions of Dissertation

In this dissertation, we consider the radar surveillance system composed of the base station, the multiple vehicles, and the bistatic radars whose antennas are mounted in each vehicle. Then, we address the problem of receiving signal level maximization at the base station, where the signal is transmitted from the vehicle and reflected by the

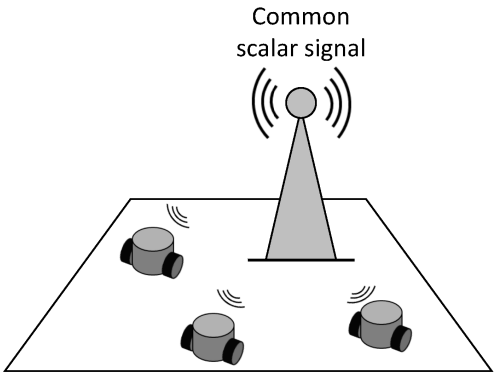

Figure 1.13: Communication of broadcast control proposed in [55, 56].

illegal drone. As mentioned in the section 1.3.4, the receiving signal level is varying for the relative positions between the vehicle and the drone due to the drone RCS. However, the system can not acquire information about the RCS. Thus, we propose a new cooperative control algorithm for multi-vehicle without such information for achieving the optimum formation in which the received signal levels at the base station are maximized. As a solution, we give a multi-agent control algorithm [54] based on the broadcast control technique recently proposed in [55, 56], where the broadcast control is a two-step switching control algorithm. By the broadcast control, the vehicles' positions are controlled with only the received signal levels at the radar and we do not need information about the drone RCS.

Since the conventional broadcast control is only applied to vehicles with omni-directional dynamics and the vehicles' velocities can not be controlled, this dissertation also proposes a new broadcast control by which both vehicle positions and velocities converge [57]. In particular, we consider the case that the vehicle dynamics is the double-integrator system and each vehicle can acquire the state of the self-velocity. In such a case, we show that the conventional two-step broadcast control can not be applied and the proposed four-step control is needed.

I prove the convergences of the algorithms under some assumptions and illustrate the effectiveness of the numerical simulations.

1.6 Outline

In Chapter 2, we explain about the conventional broadcast control for multi-vehicle proposed in [55,56]. The broadcast control system is composed of the global controller in the base station and the local controller in the vehicle. The former evaluates the objective function corresponding to the vehicle formation using the vehicle position information and broadcasts the common signal of the evaluated value to all vehicles. On the other hand, the latter receives the signal and switches the control laws by two-step. We begin with offering the problem formulation for the broadcast control. Especially, we show that the base station in the system is assumed to acquire the evaluated value of the objective function for the vehicle positions, and the assumed system in the previous works is composed of the omni-directional vehicle dynamics.

In Chapter 3, we show a new broadcast control for the anti-drone system using multi-vehicle with the antenna [54]. In the system, we assume that the base station acquires not vehicle positions' information but received signal levels of the radio waves which are transmitted by the antennas mounted in the vehicles and reflected by the illegal drones. The levels depend on the vehicle positions, illegal drone positions, and the RCS of the drones. These positions and RCS are unknown to the system. Nevertheless, we prove the convergence of the proposed broadcast control for such a system.

In Chapter 4, we also propose a broadcast control for the vehicle with the double-integrator dynamics [57]. In such dynamics, it is important to control not only the vehicle positions but also the velocities. We first show non-convergence of the velocity when using the conventional two-step local controller. We then derive the new four-step local controller and prove the convergence. We show the effectiveness of the proposed broadcast control by numerical simulations.

Chapter 2

Conventional Broadcast Control

2.1 Introduction

In the broadcast control [55, 56], the system composed of a base station and multi-vehicle is considered. The base station has an objective function, acquires the value of the function by measuring the state corresponding to the vehicle positions, and transmits the common signal to the vehicles. After receiving the signal, each vehicle moves to the direction where the value decreases by the common control law.

When considering the problem of radar signal level maximization for detecting the illegal drones explained in 1.3.4, unknown information such as RCS is included in the dynamics of the vehicle position transition and the signal propagation. In the broadcast control, however, information about the vehicle dynamics is not needed. Thus, the broadcast control may be applied to the anti-drone system and we focus on it. In this chapter, we explain the conventional broadcast control.

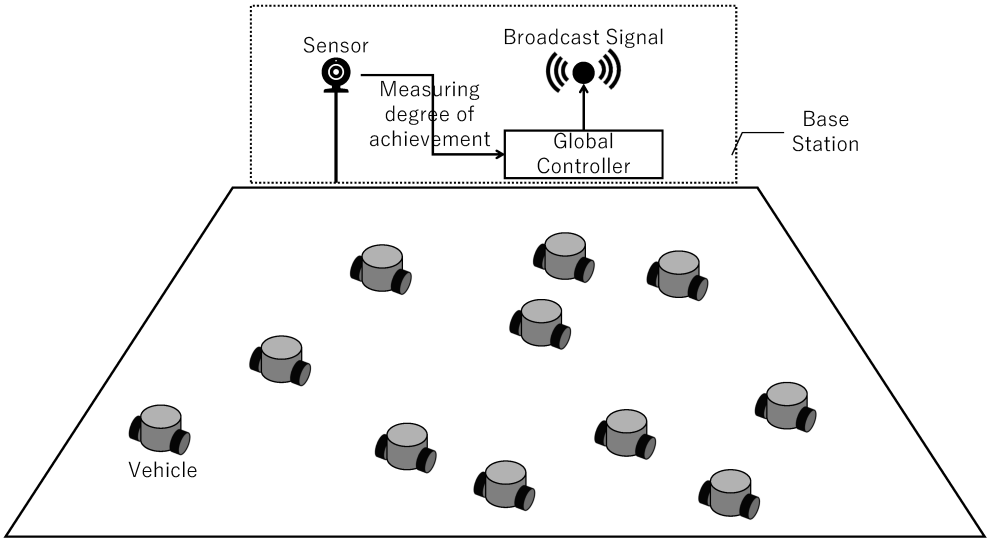

Figure 2.1: Broadcast control system.

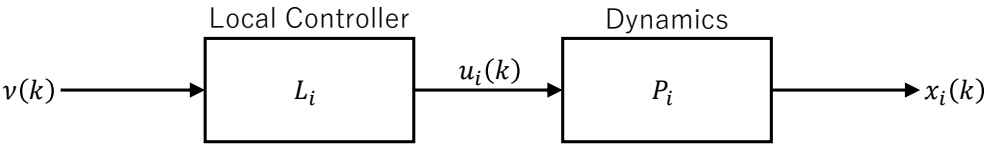

Figure 2.2: Block diagram of vehicle.

2.2 Problem Formulation

We consider the system composed of the $N \in \mathbb{N}$ vehicles on the two-dimensional plane and the base station illustrated in Figure 2.1. We show their models as follows.

Figure 2.2 illustrates the block diagram of the vehicle. The vehicle is composed of the controller L_i called "local controller" in the broadcast control literature and physical dynamics P_i. In the chapter, we assume that the physical dynamics of the vehicle is given by the omni-directional model as

$$P_i : x_i(k+1) = x_i(k) + u_i(k), \quad i = 1, 2, \ldots, N, \tag{2.1}$$

where $x_i(k) \in \mathbb{R}^2$ and $u_i(k) \in \mathbb{R}^2$ mean the position and the control input of the vehicle i, respectively. The local controller L_i is given by

$$L_i : u_i(k) = h(\nu(k), \nu(k-1), \ldots, \nu(0)), \quad i = 1, 2, \ldots, N, \tag{2.2}$$

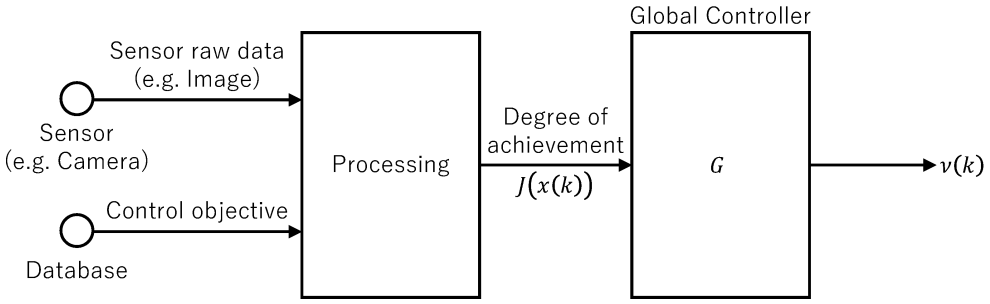

Figure 2.3: Block diagram of base station.

where $\nu(k) \in \mathbb{R}_{0+}$ means a scalar broadcast signal from the base station. We can confirm that the inputs of the local controller, that is, broadcast signals $\nu(k), \nu(k-1), \ldots, \nu(0)$ are common among all vehicles. We define the positions and the the control inputs of the vehicles as

$$x(k) = \begin{bmatrix} x_1(k) \\ x_2(k) \\ \vdots \\ x_N(k) \end{bmatrix}, \quad u(k) = \begin{bmatrix} u_1(k) \\ u_2(k) \\ \vdots \\ u_N(k) \end{bmatrix}. \tag{2.3}$$

On the other hand, Figure 2.3 illustrates the block diagram of the base station. The global controller G outputs the broadcast signal based on the evaluating result of the degree of achievement as

$$G : \nu(k) = J(x(k)) \tag{2.4}$$

where the positions of all vehicles $x(k)$ can be measured at the base station and the function $J : \mathbb{R}^{2N} \to \mathbb{R}_{0+}$ means the objective function for evaluating the difference between the current vehicle positions and the reference formation.

Problem 2.1. We consider the system composed of the equations (2.1), (2.2), and (2.4). Suppose that an objective function $J : \mathbb{R}^{2N} \to \mathbb{R}_{0+}$ is given. Find a local controller h satisfying

$$\lim_{k \to \infty} J(x(k)) = \min_{x \in \mathbb{R}^{2N}} J(x). \tag{2.5}$$

2.3 Algorithm

A solution for the problem 2.1 has been given in [55, 56] as follows:

$$h(\nu(k), \nu(k-1)) = \begin{cases} c(k)\Delta_i(k) & \text{if } k \text{ is even,} \\ u_i^{\circ}(\nu(k), \nu(k-1)) & \text{if } k \text{ is odd,} \end{cases} \tag{2.6}$$

$$\begin{aligned} u_i^{\circ}(\nu(k), \nu(k-1)) &= -c(k-1)\Delta_i(k-1) \\ &\quad -a(k-1)\frac{\nu(k)-\nu(k-1)}{c(k-1)}\Delta_i^{(-1)}(k-1) \end{aligned} \tag{2.7}$$

where $a(k) \in \mathbb{R}_{0+}$ and $c(k) \in \mathbb{R}_{0+}$ are the time-varying control gains and $\Delta_i(k) \in \mathbb{R}^2$ is the i.i.d. random variable in the local controller of the vehicle i. Additionally, $\Delta_i^{(-1)}(k) \in \mathbb{R}^2$ means the element-wise inverse of $\Delta_i(k)$. The equation (2.6) is a two-step controller which means switching alternately in the case that k is even and k is odd.

We show the mechanism of the local controller (2.6) as follows. First, from the equations (2.1),(2.2) and (2.6), the vehicles move randomly when k is even as

$$x(k+1) = x(k) + c(k)\Delta(k), \tag{2.8}$$

where

$$\Delta(k) = \begin{bmatrix} \Delta_1(k) \\ \Delta_2(k) \\ \vdots \\ \Delta_N(k) \end{bmatrix}. \tag{2.9}$$

Then, the discrete time index k is updated and k becomes odd. Next, the base station measures the value of $J(x(k))$ and broadcasts $\nu(k)$ for all vehicles. In this time, from the equations (2.4) and (2.8), the broadcast signal can be expressed as

$$\nu(k) = J\left(x(k-1) + c(k-1)\Delta(k-1)\right) \quad \text{if } k \text{ is odd.} \tag{2.10}$$

The vehicles receive $\nu(k)$ of the equation (2.10) and calculate the control input $u_i^{\circ}(\nu(k), \nu(k-1))$. By the control input, the vehicles move in the direction in which

the objective function will decrease. By the result of the two-step switching control, from the equations (2.1), (2.2), (2.6), (2.7), and (2.8), We have

$$x(k+2) = x(k) - a(k)d(k,k+1) \quad \text{if } k \text{ is even}, \tag{2.11}$$

$$d(k,l) = \frac{\nu(l)-\nu(k)}{c(k)}\Delta^{(-1)}(k), \tag{2.12}$$

where $\Delta^{(-1)}(k) \in \mathbb{R}^{2N}$ means the element-wise inverse of $\Delta(k)$. Additionally, from the equations (2.10) and (2.12), $d(k,k+1)$ can be represented by

$$d(k,k+1) = \frac{J\left(x(k)+c(k)\Delta(k)\right) - J\left(x(k)\right)}{c(k)}\Delta^{(-1)}(k) \quad \text{if } k \text{ is even}. \tag{2.13}$$

In this case, the equation

$$E\left[d(k,k+1)|x(k)\right] = \nabla J(x(k)) + \mathcal{O}(c(k)) \tag{2.14}$$

holds and $d(k,k+1)$ is the approximate value for the gradient of J [55, 56]. Therefore, the equation (2.11) can be interpreted as a stochastic gradient method and the equation (2.5) is expected to be achieved under some assumptions.

2.4 Convergence Result

In the section, we show the convergence result [55, 56] of the generlized system of the equation (2.11) by replacing $k+2$, x, Δ, and J with $k+1$, the vector $\zeta \in \mathbb{R}^{\phi}$, $\phi \in \mathbb{N}$, the random variable $\Delta_0 \in \mathbb{R}^{\phi}$, and the funtion $J_0 : \mathbb{R}^{\phi} \to \mathbb{R}_{0+}$, respectively.

We consider the system

$$\zeta(k+1) = \zeta(k) - a(k)\frac{J_0(\zeta(k)+c(k)\Delta_0(k)) - J_0(\zeta(k))}{c(k)}\Delta_0^{(-1)}(k), \tag{2.15}$$

where Δ_0 is composed of the random variable $\Delta_{0,i} \in \mathbb{R}$, $i = 1, 2, \ldots, \phi$, that is,

$$\Delta_0(k) = \begin{bmatrix} \Delta_{0,1}(k) & \Delta_{0,2}(k) & \cdots & \Delta_{0,\phi}(k) \end{bmatrix}^{\mathrm{T}} \tag{2.16}$$

and $\Delta_0^{(-1)} \in \mathbb{R}^{\phi}$ means the elementwise inverse of Δ_0.

For the system (2.15), the following result is known [55].

Lemma 2.1. In the system (2.15), we assume that the function J_0 is differentiable and there exists $\zeta^* \in \mathbb{R}^\phi$ satisfying $\nabla J_0(\zeta^*) = 0$. Then,

$$\lim_{k\to\infty} \zeta(k) = \zeta^* \quad \text{w.p.1}, \tag{2.17}$$

if the following seven conditions hold [55]:

(B1) J_0 is twice differentiable.

(B2) ζ^* is asymptotically stable equilibrium of the gradient system $\dot{\eta}(t) = -\nabla J_0(\eta(t))$ in the Lyapunov sense, where $\eta \in \mathbb{R}^\phi$.

(B3) $\lim_{k\to\infty} a(k) = 0$, $\sum_{k=0}^{\infty} a(k) = \infty$, $\lim_{k\to\infty} c(k) = 0$, and $\sum_{k=0}^{\infty}(a(k)/c(k))^2 < \infty$.

(B4) $\Delta_{0,i}(k)$, $i = 1, 2, \ldots, N$ is symmetrically distributed about zero and i.i.d. for all k and all elements. $|\Delta_{0,i}(k)| < \infty$, $|\Delta_{0,i}^{-1}(k)| < \infty$, and $|\Delta_{0,i}^{-2}(k)| < \infty$ hold w.p.1.

(B5) $E[J_0(\zeta(k) + c(k)\Delta(k))^2]$ is bounded for all $k \in \mathbb{N}$.

(B6) For a compact set $\mathbb{S}_\zeta \subseteq \mathbb{R}^\phi$ such that $\dot{\eta}(t) = -\nabla J_0(\eta(t))$ with $\zeta(0) \in \mathbb{S}_\zeta$ results in $\lim_{k\to\infty} \zeta(k) = \zeta^*$, $\zeta(k) \in \mathbb{S}_\zeta$ occurs infinitely often for almost all sample points of $\Delta_i(k)$ $(i = 1, 2, \ldots, \phi,\ k = 0, 1, \ldots)$.

(B7) $\sup_{k\in\mathbb{N}} \|\zeta(k)\| < \infty$ w.p.1.

Since the system (2.11) is given by replacing $k + 1$ with $k + 2$ in the equation (2.15), the equation (2.17) holds for the system (2.11), that is, $x(k)$ converges to a local optimum for the objective function $J(x)$ by the function of the local controller (2.6).

2.5 Numerical Simulation Results

We show some examples of the numerical simulations for conventional broadcast control. The simulation conditions are as follows: $N = 4$, $x_1(0) = [-10\ -10]^{\mathrm{T}}$,

$x_2(0) = [-10\ -9]^{\mathrm{T}}$, $x_3(0) = [-9\ -9]^{\mathrm{T}}$, $x_4(0) = [-9\ -10]^{\mathrm{T}}$, and $\Delta_i(k)$ is drawn from the Bernoulli distribution with equal probabilities in $\{-1, 1\}^2$.

Additionally, we set the time-varying control gains of the local controller as

$$a(k) = \frac{a_0}{\left(b\frac{k}{2} + 1 + a_v\right)^{a_p}}, \tag{2.18}$$

$$c(k) = \frac{c_0}{\left(b\frac{k}{2} + 1\right)^{c_p}}, \tag{2.19}$$

for the positive constants a_0, a_p, a_v, b, c_0, and c_p.

2.5.1 Formation Control

We define the objective function J in the equation (2.4) as

$$J(x) = \frac{1}{N}\left(x - x_{\mathrm{ref}}\right)^{\mathrm{T}}\left(x - x_{\mathrm{ref}}\right), \tag{2.20}$$

$$x_{\mathrm{ref}} = \begin{bmatrix} x_{1,\mathrm{ref}}^{\mathrm{T}} & x_{2,\mathrm{ref}}^{\mathrm{T}} & x_{3,\mathrm{ref}}^{\mathrm{T}} & x_{4,\mathrm{ref}}^{\mathrm{T}} \end{bmatrix}^{\mathrm{T}}, \tag{2.21}$$

where $x_{i,\mathrm{ref}} \in \mathbb{R}^2$ is the reference position of the vehicle i. The objective function $J(x)$ is twice differentiable with x and satisfies the condition in Lemma 2.1. We illustrate that x approaches to the reference formation x_{ref} by the conventional local controller (2.2) and (2.6).

We set the parameters in the equations (2.18) and (2.19) as $a_0 = 3 \times 10^{-3}$, $c_0 = 10^{-4}$, $a_p = 7.0 \times 10^{-1}$, $c_p = 1.6 \times 10^{-1}$, $a_v = 10^{-6}$, $b = 10^{-5}$, so that the parameters $a(k)$ and $c(k)$ satisfy the condition in Lemma 2.1. The reference positions are as follows: $x_{1,\mathrm{ref}} = [-6\ -6]^{\mathrm{T}}$, $x_{2,\mathrm{ref}} = [-6\ -6]^{\mathrm{T}}$, $x_{3,\mathrm{ref}} = [6\,6]^{\mathrm{T}}$, and $x_{4,\mathrm{ref}} = [6\ -6]^{\mathrm{T}}$.

Figure 2.4 and 2.5 illustrate the simulation result. Figure 2.4 depicts the vehicles positions $x_i(k)$, $i = 1, 2, \ldots, N$ in the two-dimensional plane. In the figure, the symbols $\bigcirc$, $\triangle$, $\square$, $\times$ with line show each vehicle position at time k and the previous trajectory to the past 5000 samples, respectively. On the other hand, the other four symbols + mean the positions corresponding to the reference formation x_{ref} in the equation (2.21).

From Figure 2.4, we can find that vehicle positions approach the reference formation at $k = 4000$ and equilibrate at the same place after that. Then, from Figure 2.5,

which shows the time series of the objective function and vehicle positions, we see that the objective function approaches to 0 and positions are almost equal to 6 or -6 at $k = 5000$, which matches Figure 2.4. Thus, these results show that Problem 2.1 is solved by the local controller (2.2) and (2.6).

2.5.2 Coverage Control

We also evaluate the effectiveness of conventional broadcast control for the other objective functions and consider the coverage problem [58]. The coverage means locating the vehicles in the bounded area $W \subset \mathbb{R}^2$ without any explicit reference positions so that the vehicles' occupied areas are equal [55]. Then, we divide the bounded area into a grid. The objective function corresponding to the problem can be represented by

$$J(x) = \frac{1}{L} \sum_{l=1}^{L} \min_{i \in \mathcal{N}} \|w_l - x_i\|^2, \tag{2.22}$$

where $w_l \in W$, $l = 1, 2, \ldots, L$ is the l th corner position of the grid in the bounded area, L is the number of corners, and $\mathcal{N} = \{1, 2, \ldots, N\}$. As illustrated in Figure 2.6, we set the bounded area and the number of corners as $W := [-12, 12] \times [-12, 12]$ and $L = 25^2 = 625$, respectively. Thus, the corner positions of the grid are given by

$$w_1 = \begin{bmatrix} -12 \\ -12 \end{bmatrix}, \quad w_2 = \begin{bmatrix} -12 \\ -11 \end{bmatrix}, \quad \ldots, \quad w_{625} = \begin{bmatrix} 12 \\ 12 \end{bmatrix}. \tag{2.23}$$

The region corresponding to the set $\{w_l : \|w_l - x_i\| \leq \|w_l - x_j\|, \forall j \in \{1, 2, \ldots, N\}\}$ is called Voronoi region for the position x_i [58]. When the vehicles' positions are equal to the local optimum of the objective function (2.22), the areas of the Voronoi regions are equal.

The objective function (2.22) is known to be differentiable with x [58] but unclear about twice differentiability. We evaluate the effectiveness of such an objective function. About the parameters in the local controller, we set the same values as the case of the equation (2.20) except for a_0. We set $a_0 = 10^{-1}$ in the simulation.

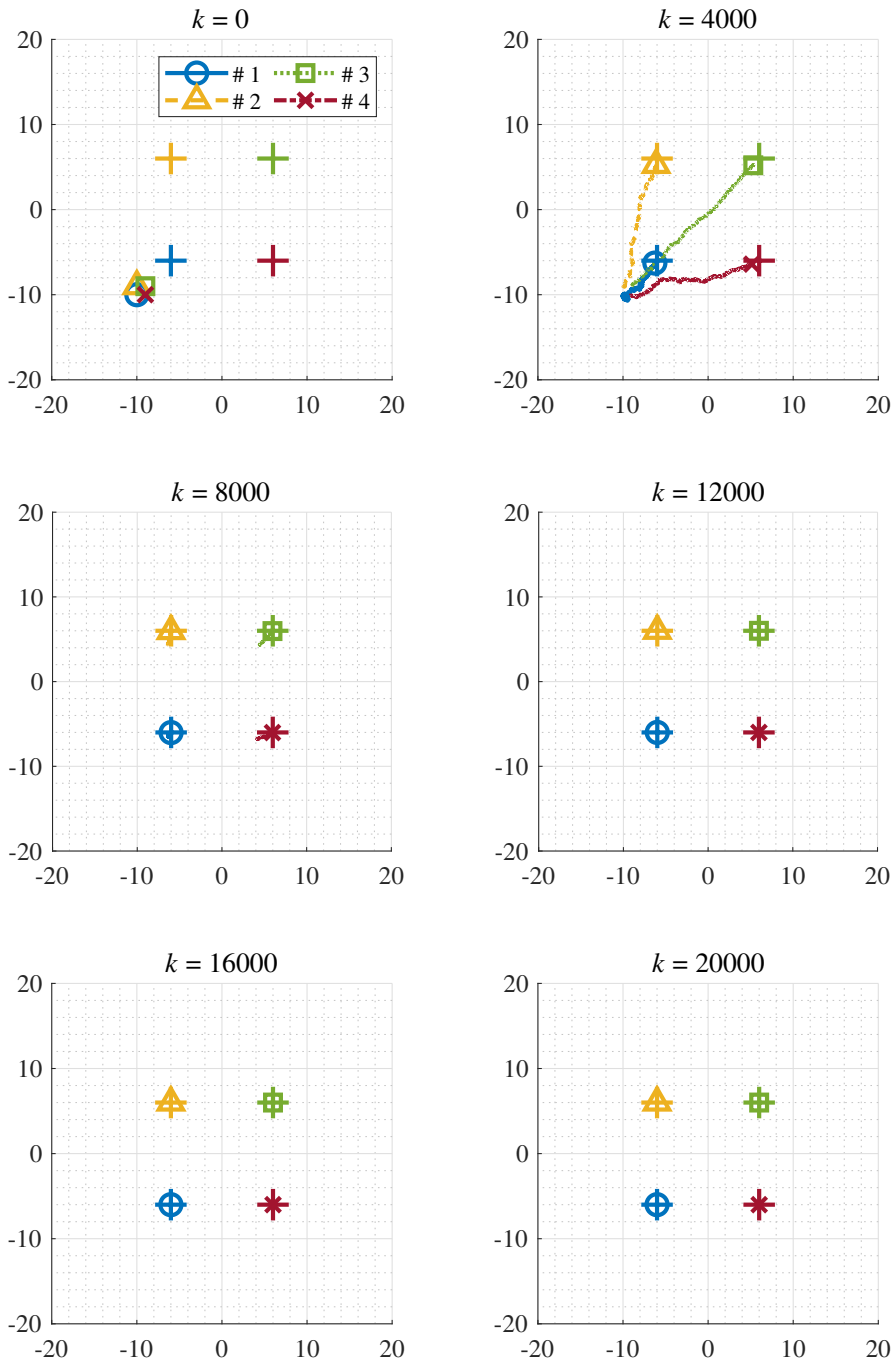

Figure 2.4: Vehicle positions transition in two-dimensional plane for objective function (2.20).

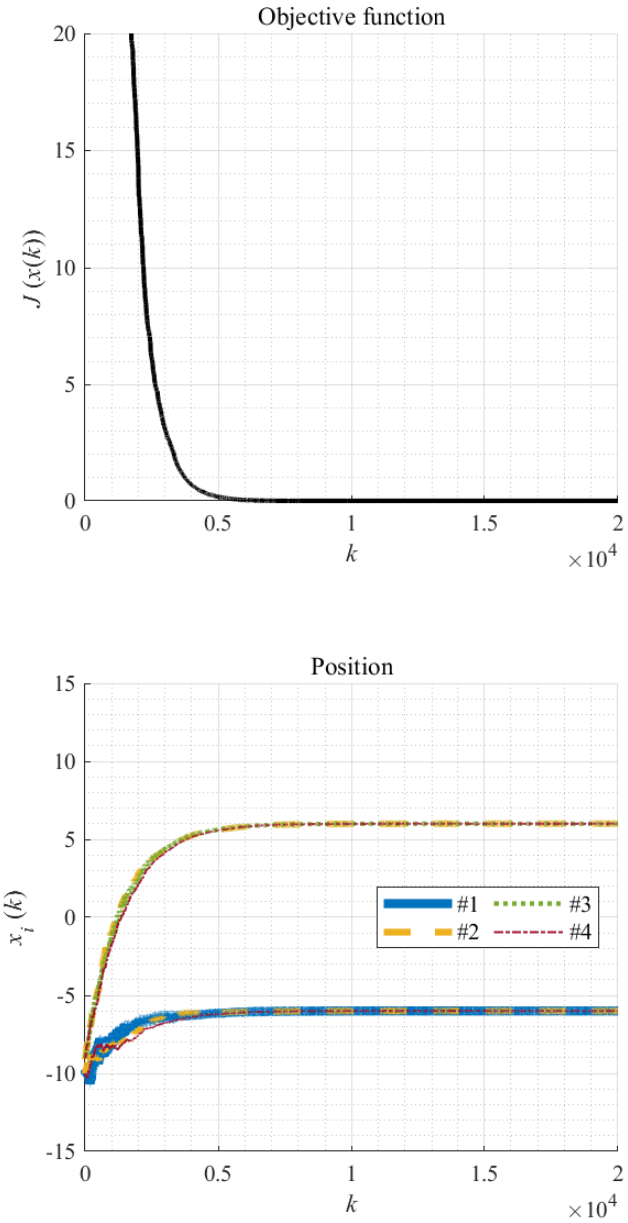

Figure 2.5: Time series of objective function (2.20) and vehicles positions.

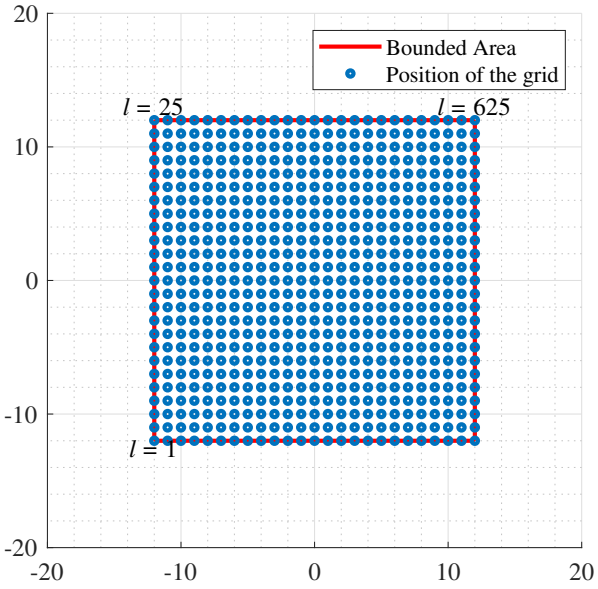

Figure 2.6: Bounded area and corner positions of grid in objective function (2.22) on two-dimensional plane.

Figure 2.7 and 2.8 illustrate the simulation result. Figure 2.7 depicts the vehicles positions $x_i(k)$, $i = 1, 2, \ldots, N$ by the almost same manner of Figure 2.4. In the figure, the bounded area and the borders of the Voronoi regions are also illustrated by the rectangle and straight-line symbols, respectively. From the figure, we see that the four vehicles converge to the positions for which the areas of Voronoi regions are almost equal in the bounded area W (the bounded area is divided into almost equal quarters by the borders of the Voronoi regions). Figure 2.8 illustrates the time series of the objective function and the vehicle positions same as Figure 2.5. We can confirm that the objective function and positions converge to certain values. Note that the minimum value of the objective function (2.22) may not be not zero.

2.6 Conclusion

In this chapter, we have reviewed the conventional broadcast control proposed in [55, 56]. Especially, we have shown the assumed system model in the control, the

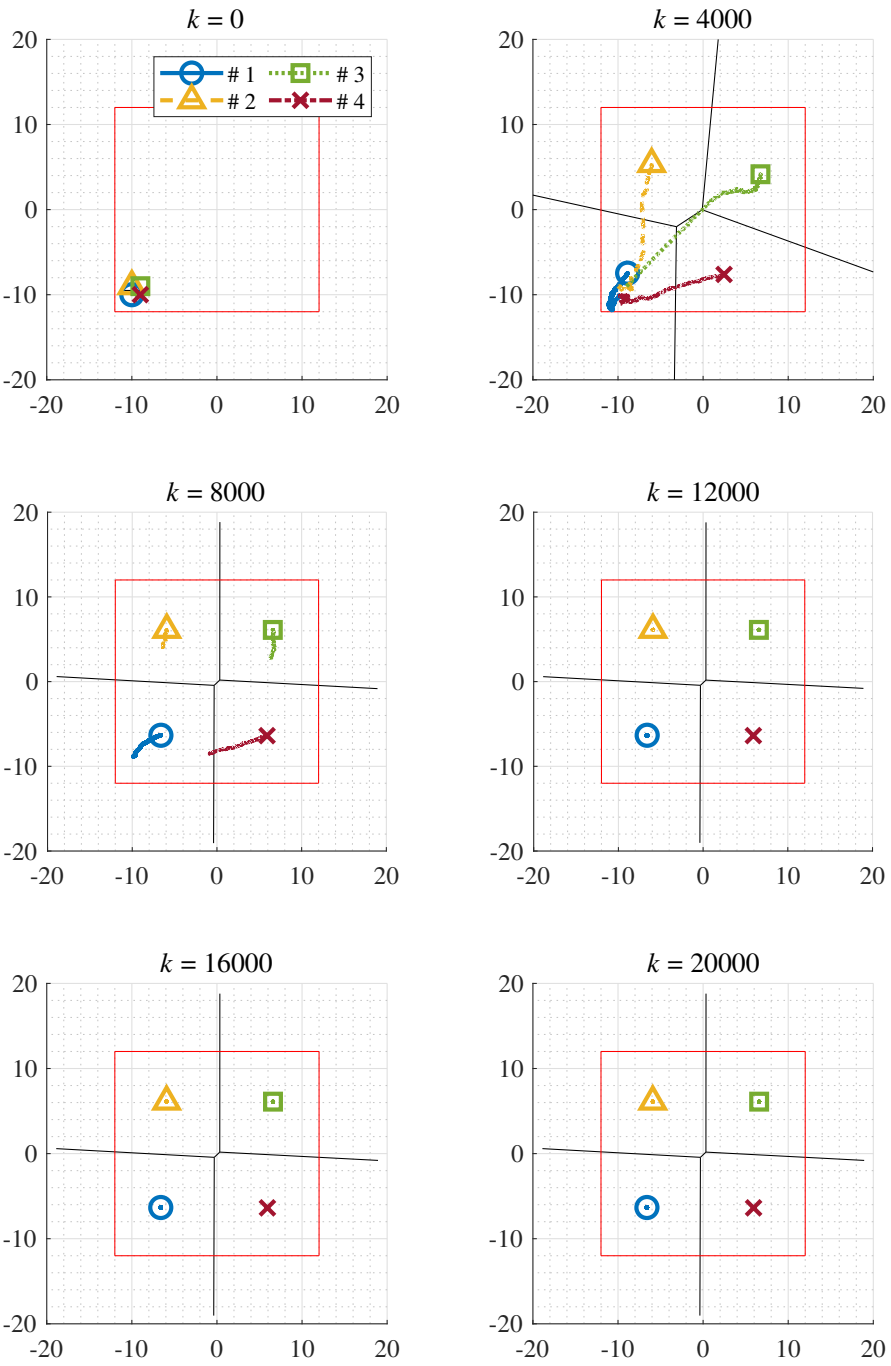

Figure 2.7: Vehicle positions transition in two-dimensional plane for objective function (2.22).

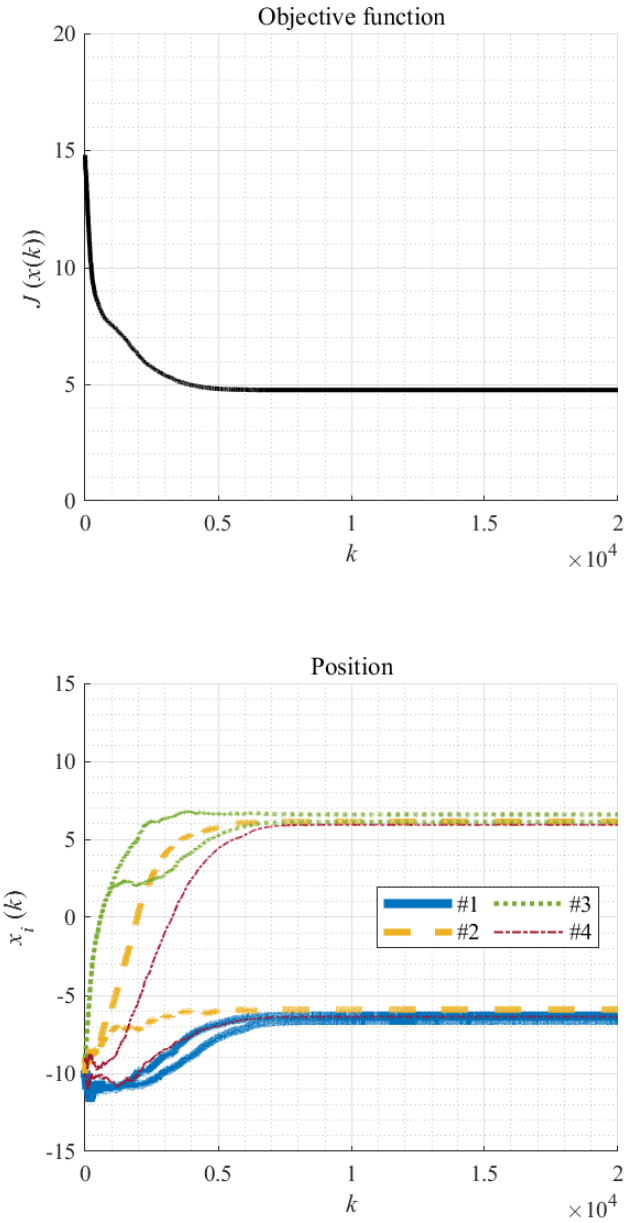

Figure 2.8: Time series of objective function (2.22) and vehicles positions.

algorithms, the convergence result, and some numerical simulation results. In the algorithm, the base station and the vehicles only need the value of the objective function and the common signal from the base station, respectively. This characteristic is convenient for the system including the unknown dynamics. However, the case that the vehicle dynamics is the single-integrator system has only been studied. Thus, we propose a new radar surveillance system using the broadcast control against the illegal drone with unknown RCS and the new broadcast control for the case that the vehicle dynamics is the double-integrator system.

Chapter 3

Broadcast Control of Radar Surveillance Systems for Unexpected Drones

3.1 Introduction

In this chapter, we propose a new broadcast control for the radar-surveillance system. As the conventional broadcast control [55, 56], the system for the proposed one is also composed of the base station and multiple vehicles. In the proposed control, however, the base station receives radio waves that are transmitted from the vehicles and reflected by the illegal drones (called intruders in this chapter). Thus, the system is regarded as the bistatic radar with multiple vehicles which have a role as the transmission antenna. But the conventional radar-surveillance system such as [30] has only the motionless transmission antenna and the RCS is unknown for the system and may lose the intruders. In the system, therefore, we address the problem of steering vehicles to a formation maximizing the levels of the radar echo signals at the receiving antenna in the base station. Especially, we propose the algorithm for the

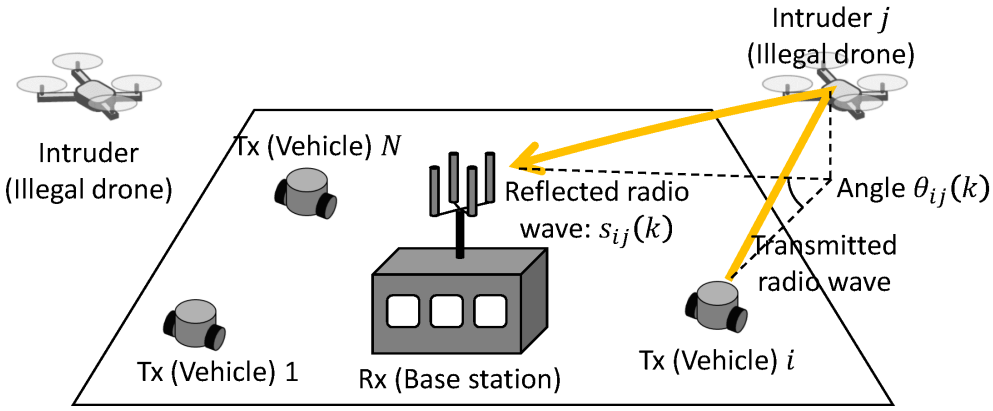

Figure 3.1: Proposed surveillance system using antenna-equipped vehicles for detecting intruders.

system with the unknown radio waves propagation due to the RCS. The broadcast control algorithm can work only information about the objective function and the broadcast signal calculated with the output of the objective function. Additionally, the algorithm does not need information about the dynamics in operation. Thus, we focus on the algorithm for the system with the unknown dynamics such as RCS.

3.2 Problem Forumlation

We consider the surveillance system for detecting $M \in \mathbb{N}$ intruders as shown in Fig. 3.1 [54]. This system is composed of N vehicles denoted by Tx i and the base station denoted by Rx.

Vehicles of Transmission Antenna (Tx): Vehicles Tx i $(i = 1, 2, \ldots, N)$ move on the ground and transmit radio waves for detecting the intruders. The vehicles cannot localize their positions in the global coordinate flame, but they can receive a control signal from Rx. We assume that each Tx stays on-site during the transmission of radio waves, which guarantees that the Doppler shift caused by Tx does not occur. Thus, the Doppler shift of the received signal at the base station is only associated with the intruders' movement and the base station

can ignore the signal directly arriving from Tx. In addition, we also assume that the base station can calculate the sum of the signals' levels without radio frequency interference, that is, the frequencies of Tx's transmitted signals are different from each other, and the base station distinguishes the transmitted signals.

Base Station (Rx): The base station Rx is placed on the fixed location, while it receives the signals transmitted by Tx i $(i = 1, 2, \ldots, N)$ and reflected by the intruders j $(j = 1, 2, \ldots, M)$. Rx detects the intruder through the received signal level $s_{ij}(k) \in \mathbb{R}$ $(i = 1, 2, \ldots, N, j = 1, 2, \ldots, M)$, which is transmitted from Tx i and reflected by the intruder j, and the Doppler shift. Note that Rx can receive $s_{ij}, (i = 1, 2, \ldots, N, j = 1, 2, \ldots, M)$ at the same time because the different frequencies and angles are used to transmit them. Furthermore, Rx has an array antenna and can estimate the number of the intruders M by the arrival angles differences of received signals using array signal processing such as Capon algorithm [59]. Based on the received signals, Rx transmits the control signal $\nu(k)$ to all of Tx in an indiscriminate manner. Thus, Rx has the role of the central controller in the proposed surveillance system. When all the signal levels are low and the Doppler shifts are not detected, Rx detects no intruder and does not transmit the control signal to Tx. Without loss of generality, we assume that Rx is placed at the origin in the global coordinate frame.

Intruder: In Fig. 3.1, we assume the intruders are hovering in the air at the same altitude for illegal fixed-point photography.

The block diagram of Tx i is illustrated in Fig. 3.2. Tx i is composed of the physical dynamics P_i, the local controller L_i, and signal transmission D_{ij} to Rx. The physical dynamics and the function of the local controller of Tx i are given by the equation (2.1) and (2.6), respectively. The input of the local controller $\nu(k)$ is broadcasted by Rx, and the output is $u_i(k)$, which is applied to P_i. The signal

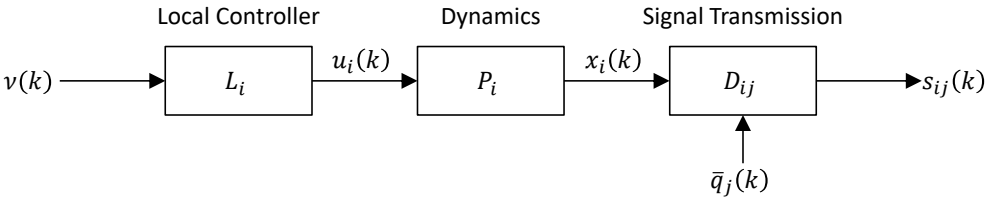

Figure 3.2: Block diagram of Tx i.

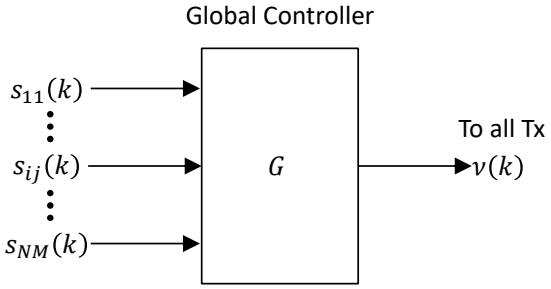

Figure 3.3: Block diagram of Rx.

transmission D_{ij} is modeled as

$$D_{ij} : s_{ij}(k) = r(x_i(k), \bar{q}_j(k)) \tag{3.1}$$

where $\bar{q}_j(k) \in \mathbb{R}^3$ is the three-dimensional position of the intruder j composed of the position on the 2-D plane $q_j(k) \in \mathbb{R}^2$ and the altitude[1] $q_{zj}(k) \in \mathbb{R}_+$, that is, $\bar{q}_j(k) = \begin{bmatrix} q_j^{\mathrm{T}}(k) & q_{zj}(k) \end{bmatrix}^{\mathrm{T}}$ and r is the function representing the signal level for the intruder position $\bar{q}_j(t)$ and the Tx i position $\begin{bmatrix} x_i^{\mathrm{T}}(k) & 0 \end{bmatrix}^{\mathrm{T}}$, which is assumed to be unknown but may depend on the distance between Tx i and the intruder j, i.e.,

$$d(x_i(k), \bar{q}_j(k)) = \left\| \begin{bmatrix} x_i^{\mathrm{T}}(k) & 0 \end{bmatrix} - \bar{q}_j(k) \right\|, \tag{3.2}$$

and the angle $\theta_{ij}(k) \in \mathbb{R}$ illustrated in Fig. 3.1. Since the intruders are assumed to be hovering in the air, we can regard $\bar{q}_j(k)$ $(j = 1, 2, \ldots, M)$ as constant parameters and we can rewrite $d_j(x_i(k)) = d(x_i(k), \bar{q}_j(k))$ and D_{ij} as

$$D_{ij} : s_{ij}(k) = r_j(x_i(k)). \tag{3.3}$$

[1]The altitude means the height in the 3-D space. From the assumption of the intruder's hovering, $q_{zj}(k) > 0$.

On the other hand, the block diagram of Rx is illustrated in Fig. 3.3, which receives the signals $s_{ij}(k)$ $(i = 1, 2, \ldots, N, j = 1, 2, \ldots, M)$ and broadcasts the same signal $\nu(k)$ to Tx i $(i = 1, 2, \ldots, N)$. This is given by

$$G : \nu(k) = f(s_{11}(k), \ldots, s_{NM}(k)) \tag{3.4}$$

where f is a function.

The objective of this surveillance system is to move Tx i $(i = 1, 2, \ldots, N)$ maximizing the collective signal level of Rx for detecting all the intruders. The collective signal level is quantified as the objective function

$$J(s_{11}, \ldots, s_{NM}) = \sum_{j=1}^{M} \frac{1}{\beta_j(s_{1j}, s_{2j}, \ldots, s_{Nj})} \tag{3.5}$$

where

$$\beta_j(s_{1j}, s_{2j}, \ldots, s_{Nj}) = \sum_{i=1}^{N} \log s_{ij} \tag{3.6}$$

which corresponds to the signal level capturing the intruder j illustrated in Figure 3.4. The inverses of $\beta_j(s_{1j}, s_{2j}, \ldots, s_{Nj})$ represent the signal weaknesses to detect the intruders j $(j = 1, 2, \ldots, M)$, and the objective function in (3.5) corresponds to the average of them (more precisely, constant multiplication of the average). In this sense, the signal level at Rx is maximized by minimizing the objective function.

Although the base station measures the β_j with the signal levels s_{ij} by the equation (3.6), the signal level J eventually depends on the positions x of the Tx vehicles. To clarify this dependency, we introduce

$$\tilde{J}(x) = \sum_{j=1}^{M} \frac{1}{\tilde{\beta}_j(x)}, \tag{3.7}$$

where

$$\tilde{J}(x) \triangleq J(r_1(x_1), r_2(x_1), \ldots, r_M(x_N)) \tag{3.8}$$

and

$$\tilde{\beta}_j(x) \triangleq \beta_j(r_1(x_1), r_2(x_1), \ldots, r_M(x_N)). \tag{3.9}$$

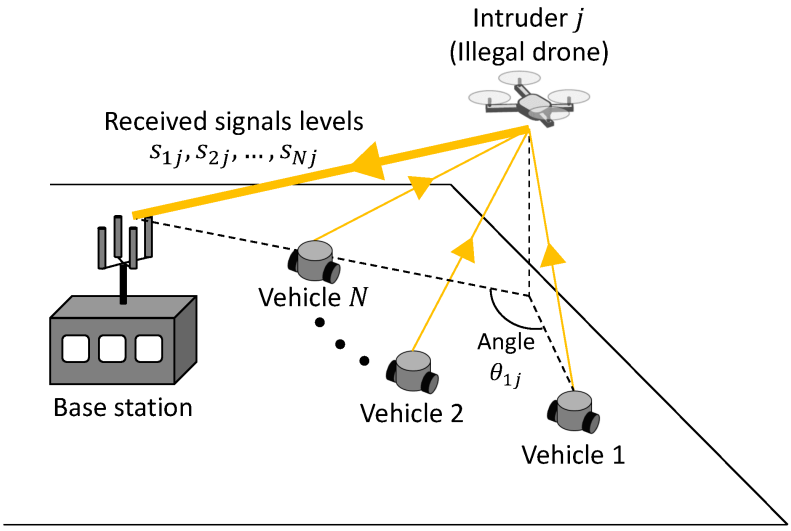

Figure 3.4: Signal level capturing intruder j.

From (3.3), (3.5), and (3.6), it is clear that $\tilde{J}$ is equivalent to J. Note that the global controller in the base station uses x for measuring J as like depicted in Fig. 3.3. Thus, we utilize s_{ij} and x as the input of the function in the discussion about development of the controller and convergence analysis, respectively.

Then our problem is formulated as follows.

Problem 3.1. Consider the above surveillance system. Assume that the model of signal transmission, i.e., r, is unknown and the intruders are hovering in the air (i.e., the third elements of $\bar{q}_j(k)$ $(j = 1, 2, \ldots, M)$ corresponding to the altitudes are constant). Find f such that $\lim_{k\to\infty} \tilde{J}(x(k))$ is equal to the minimum value of $\tilde{J}(x)$ with respect to $x_1, x_2, \ldots, x_N$.

Three remarks are given for Problem 3.1. First, the movement cost, e.g., the moving distance, should be taken into account in practice. For simplicity, it is omitted in Problem 3.1, whereas the solution is useful for wired Tx vehicles, to which power is supplied via a long cable [60]. Second, in the previous work [55,56], a general form of the objective function J has been addressed. On the other hand, this dissertation proposes a specific J to quantify the signal level in an anti-drone surveillance system. In

this sense, the objective function J is originally proposed in this dissertation. Finally, the number of intruders is assumed to be known in the problem. The assumption is reasonable when the number is estimated by using an array antenna in Rx before applying the solution to Problem 3.1.

3.3 Proposed Objective Function

In this section, we propose a solution to Problem 3.1 based on the result of the broadcast control established in [55, 56].

The function f in the equation (3.4) is given by

$$f(s_{11}(k), \dots, s_{NM}(t)) = J(s_{11}(k), \dots, s_{NM}(k)). \tag{3.10}$$

$\Delta_i(k)$ $(i = 1, 2, \dots, N,\ k = 0, 1, \dots)$ in (2.6) are drawn from the Bernoulli distribution with outcome ± 1 and equal probabilities. The control gains $a(k)$ and $c(k)$ are given by the same function as (2.18) and (2.19).

The proposed algorithm given by (2.2), (2.6), (3.4), and (3.10) is a solution to Problem 3.1 under some assumptions.

3.4 Convergence Analysis

We prove the convergence of the proposed algorithm in radar surveillance.

Theorem 3.1. For the radar-based surveillance system composed of (2.1), (3.3), (2.2), (2.6), and (3.4), let the objective function $\tilde{J}(x) : \mathbb{R}^{2N} \to \mathbb{R}_{0+}$ be given by (3.7) and let G be given by (3.10). We assume that

(A1) $\tilde{\beta}_j(x)$ $(j = 1, 2, \dots, M)$ are twice differentiable with x and $\tilde{J}(x)$ is differentiable with x,

(A2) there exists a vector $x^* \in \mathbb{R}^{2N}$ satisfying $\nabla \tilde{J}(x^*) = 0$ and is an asymptotically stable equilibrium of the gradient system $\dot{\eta}(t) = -\nabla \tilde{J}(\eta(t))$, where the stability is in the Lyapunov sense,

(A3) for a compact set $\mathbb{S} \subseteq \mathbb{R}^{2N}$ such that $\dot{\eta}(t) = -\nabla\tilde{J}(\eta(t))$ with any $\eta(0) \in \mathbb{S}$ results in $\lim_{t\to\infty} \eta(t) = x^*$, $x(k) \in \mathbb{S}$ occurs infinitely often for almost all sample points of $\Delta_i(k)$ $(i = 1, 2, \ldots, N \quad \text{and} \quad k = 0, 1, \ldots)$,

(A4) $x(0)$ is set in the circle whose center is equal to 0 (the position of Rx) and whose radius is equal to the finite communicable distance with Rx and $\sup_{k\in\mathbb{N}} \|x(k)\| < \infty$ w.p.1,

(A5) About the parameters in (2.18) and (2.19), $a_p \leq 1$ and $a_p - c_p > 0.5$.

Then $x(k)$ converges to a solution to the equation $\nabla\tilde{J}(x) = 0$ w.p.1.

Proof. Since the objective function J is equivalent to $\tilde{J}$ as mentioned above, we have

$$J(s_{11}(k), \ldots, s_{NM}(k)) = \tilde{J}(x(k)) \tag{3.11}$$

from (3.3) and (3.8). Then we can rewrite the signal $\nu(k)$ as

$$\nu(k) = \tilde{J}(x(k)), \tag{3.12}$$

which is the same form as $\nu(k)$ in the system in Problem 2.1. Therefore, the system in Problem 3.1 is in the same class as the system in Problem 2.1. Thus, we prove that the seven conditions (B1) to (B7) in Lemma 2.1 hold under (A1) - (A5).

(B1) The objective function (3.7) is twice differentiable with $x(k)$ because $\tilde{\beta}_j(x)$ is assumed to be twice differentiable with respect to x in (A1).

(B3) The condition holds from (2.18), (2.19) and (A5).

(B4) The condition holds because $\Delta_i(k)$ $(i = 1, 2, \ldots, N,\ k = 0, 1, \ldots)$ in (2.6) are random variable drawn from the Bernoulli distribution with equal probabilities in $\{-1, 1\}^2$.

(B5) Since (B4) holds and (A4) is assumed, the condition also holds.

Finally, (B2), (B6), and (B7) are straightly obtained from (A2), (A3), and (A4), respectively. Thus, Theorem follows from Lemma 2.1. □

From the theorem, we can confirm that the vehicles can arrive at the locally optimal positions for the objective function (3.7) by the proposed surveillance system only with the received signal level s_{ij}. This means that even if a nonlinear operator for the positions such as the function (3.3) is included in the system, the vehicles' positions are converged to the locally optimal values by the broadcast control technique under some assumptions shown in the theorem, which is the difference from the previous work [55, 56].

In our problem setting, Assumptions (A1) and (A2) are not so restrictive. This can be explained by using a typical model of the signal transmission r_j. From the radar equation [61], we have

$$r_j(x_i) = R_j \frac{\sigma_j(x_i)}{d_j^2(x_i)} \tag{3.13}$$

for the RCS $\sigma_j(x_i) \in \mathbb{R}_+$ of the intruder j, which is the coefficient for the reflection intensity of radio waves on the intruder's surface, and

$$R_j = \frac{\Gamma \lambda^2}{(4\pi)^3 \|\bar{q}_j\|^2} \tag{3.14}$$

where $\Gamma \in \mathbb{R}_+$ and $\lambda \in \mathbb{R}_+$ are transmission power and the wavelength of the received signal, respectively. Note that some types of $\sigma_j(x_i)$ are known to be a concave function [62]. Then the following result is obtained.

Corollary 3.1. For the system in Theorem 3.1, assume that the signal transmission model $r_j(x_i)$ is given by (3.13) and (3.14). If the following conditions are satisfied, (A1) and (A2) hold.

(a) (A4) holds.

(b) $q_{zj} > \|x_i(k) - q_j\|$ and $R_j \geq \|p_i(k) - q_j\|^2 + q_{zj}^2$ for all $k \in \{0, 1, \dots\}$ (note that $\|x_i(k) - q_j\|$ is bounded w.p.1 under (A4)).

(c) $\sigma_j(x_i)$ is concave and twice differentiable.

Proof. In the following, we prove that the assumptions (A1) and (A2) in Theorem 3.1 hold.

(A1) The denominator in (3.13) $d_j^2(x_i)$ is clearly twice differentiable with x_i. Thus, $r_j(x_i)$ is twice differentiable with x_i because both the numerator and the denominator in (3.13) are twice differentiable. Therefore, $\tilde{\beta}_j(x)$ is also twice differentiable with x from the equations (3.3), (3.6), and (3.9) and $\tilde{J}(x)$ is similarly differentiable with x from the equation (3.7).

(A2) From Lyapunov's indirect method, when the twice differentiation of $\tilde{J}$ with x is positive definite, the gradient system $\dot{\eta}(t) = -\nabla\tilde{J}(\eta(t))$ is stable. Thus, we prove that $(\partial^2\tilde{J}(x))/(\partial x^2) > 0$. From the equation (3.7), we have

$$\frac{\partial^2\tilde{J}(x)}{\partial x^2} = \sum_{j=1}^{M} \frac{1}{\tilde{\beta}_j^3(x)} \left(2\left(\frac{\partial\tilde{\beta}_j(x)}{\partial x}\right)\left(\frac{\partial\tilde{\beta}_j(x)}{\partial x}\right)^{\mathrm{T}} - \tilde{\beta}_j(x)\frac{\partial^2\tilde{\beta}_j(x)}{\partial x^2} \right) \tag{3.15}$$

and the first term is positive semi-definite. Hence, $(\partial^2\tilde{J}(x))/(\partial x^2) > 0$ and the gradient system is stable if $(\partial^2\tilde{\beta}_j(x))/(\partial x^2) < 0$. From the equations (3.3), (3.6), (3.9), and (3.13), we have

$$\tilde{\beta}_j(x) = \sum_{i=1}^{N} \log R_j \frac{\sigma_j(x_i)}{d_j^2(x_i)} = \sum_{i=1}^{N} \left(\log R_j + \log\sigma_j(x_i) - \log d_j^2(x_i) \right). \tag{3.16}$$

The first term $\log R_j$ is a constant value. The second term $\log\sigma_j(x_i)$ is concave from the concavity assumption of $\sigma_j(x_i)$ and (C2) in Lemma A.1 (Appendix). Hence, $(\partial^2\tilde{\beta}_j(x))/(\partial x^2) < 0$ from (C1) in Lemma A.1 if the twice differentiation of $\log d_j^2(x_i)$ with x is positive definite. The twice differentiation can be written as

$$\frac{\partial^2 \log d_j^2(x_i)}{\partial x^2} = \frac{1}{d_j^4(x_i)} A_j(x_i) \tag{3.17}$$

where

$$\begin{aligned} A_j(x_i) &= \frac{\partial^2 d_j^2(x_i)}{\partial x^2} d_j^2(x_i) - \left(\frac{\partial d_j^2(x_i)}{\partial x}\right)\left(\frac{\partial d_j^2(x_i)}{\partial x}\right)^{\mathrm{T}} \\ &= 4B_j(x_i) + 2\left(q_{zj}^2 - \|e(x_i, q_j)\|^2\right)\bar{I}_i^{\mathrm{T}}\bar{I}_i, \end{aligned} \tag{3.18}$$

$$B_j(x_i) = \bar{I}_i^{\mathrm{T}}\left(e^{\mathrm{T}}(x_i, q_j)e(x_i, q_j)I_2 - e(x_i, q_j)e^{\mathrm{T}}(x_i, q_j)\right)\bar{I}_i, \tag{3.19}$$

$$e(x_i, q_j) = x_i - q_j, \tag{3.20}$$

$$\bar{I}_i = \begin{bmatrix} 0_{2\times(2i-2)} & I_2 & 0_{2\times(2M-2i)} \end{bmatrix}. \tag{3.21}$$

The quadratic form of the matrix $B_j(x_i)$ can be written as

$$\begin{aligned} v^{\mathrm{T}} B_j(x_i) v &= v^{\mathrm{T}} \bar{I}_i^{\mathrm{T}} \left(e^{\mathrm{T}}(x_i, q_j) e(x_i, q_j) I_{2\times 2} - e(x_i, q_j) e^{\mathrm{T}}(x_i, q_j) \right) \bar{I}_i v \\ &= \left(e^{\mathrm{T}}(x_i, q_j) e(x_i, q_j) \right) \left(v^{\mathrm{T}} \bar{I}_i^{\mathrm{T}} \bar{I}_i v \right) - \left(v^{\mathrm{T}} \bar{I}_i^{\mathrm{T}} e(x_i, q_j) \right) \left(e^{\mathrm{T}}(x_i, q_j) \bar{I}_i v \right) \\ &= \|e(x_i, q_j)\|^2 \|\bar{I}_i v\|^2 - \left(e^{\mathrm{T}}(x_i, q_j) \bar{I}_i v \right)^2 \\ &= \left(\|e(x_i, q_j)\| \|\bar{I}_i v\| + e^{\mathrm{T}}(x_i, q_j) \bar{I}_i v \right) \\ &\quad \times \left(\|e(x_i, q_j)\| \|\bar{I}_i v\| - e^{\mathrm{T}}(x_i, q_j) \bar{I}_i v \right) \geq 0, \end{aligned} \tag{3.22}$$

where $v \in \mathbb{R}^{2N}$. On the other hand, $2\left(q_{zj}^2 - \|e(x_i, q_j)\|^2\right) \bar{I}_i^{\mathrm{T}} \bar{I}_i$ in (3.18) is positive definite from the assumption that $q_{zj} > \|x_i(k) - q_j\|$ for all $k \in \{0, 1, \dots\}$. Thus, the matrix $A_j(x_i)$ and the twice differentiation of $\log d_j^2(x_i)$ are also positive definite from (3.17). Therefore, we can confirm that $(\partial^2 \tilde{\beta}_j(x))/(\partial x^2) < 0$, $(\partial^2 \tilde{J}(x))/(\partial x^2) > 0$, and the gradient system $\dot{\eta}(t) = -\nabla \tilde{J}(\eta(t))$ is stable.

□

3.5 Numerical Simulation

This section evaluates the proposed method by numerical simulation.

Consider the surveillance system with the proposed controller, where $N = 3$, $M = 3$, and the control gains are given by (2.18) and (2.19) for $a_0 = 10^1$, $c_0 = 10^{-1}$, $a_v = 10^{-6}$, $a_p = 0.70$, $c_p = 0.16$, and $b = 10^{-5}$. These parameters are given to satisfy the condition (B3) in Theorem 3.1. The signal transmission models D_{ij} $(i = 1, 2, \dots, N, j = 1, 2, \dots, M)$ are given by the radar equation (3.13), where $\Gamma = 2.0 \times 10^{15}$ and $\lambda = 0.03$.

Here, we consider the following two cases of the RCS such that the assumptions about differentiability and concavity in the corollary 3.1 are satisfied:

1.

$$\sigma(x_i(k), q_j(k)) = 1. \tag{3.23}$$

2.

$$\sigma(x_i(k), q_j(k)) = \frac{\pi}{(1 + \cos\theta_{ij}(k) + \epsilon)^2}, \tag{3.24}$$

where $\epsilon = 10^{-5}$ is given for prevention of division by zero.

The former is the simplest model for which $s_{ij}(k)$ is maximized when a Tx i goes to immediately below the intruder j. The latter corresponds to the model that the intruder's surface is regarded as an elliptic paraboloid including the unknown nonlinear factor of the angles $\theta_{ij}(k)$ $(i = 1, 2, \ldots, N, j = 1, 2, \ldots, M)$ [62].

Note that we cannot use the above models (3.23) and (3.24) in D_{ij} for designing the controller but we can use the instantaneous values $s_{ij}(k)$ $(i = 1, 2, \ldots, N)$.

Figure 3.5 and 3.6 show the result for Case (i) where the altitudes of the intruders are 10m. The former illustrates the snapshots of the positions of Tx i $(i = 1, 2, \ldots, N)$ and the intruders in $\mathbb{R}^2$. The latter depicts the trajectories of Tx i $(i = 1, 2, \ldots, N)$ and the time evolution of the objective function J. In the figures, the circles, crosses, and squares indicate Tx i, Rx, and the intruders, respectively. As illustrated in Fig. 3.5,

$$x_1(0) = \begin{bmatrix} -20 & -100 \end{bmatrix}^{\mathrm{T}}, \tag{3.25}$$

$$x_2(0) = \begin{bmatrix} -40 & -100 \end{bmatrix}^{\mathrm{T}}, \tag{3.26}$$

$$x_3(0) = \begin{bmatrix} -60 & -100 \end{bmatrix}^{\mathrm{T}}. \tag{3.27}$$

We see that all Tx are approaching nearby the intruders as time passes. At $k = 33333$, Tx vehicles are separately going to each intruder without explicit target allocation. Finally, all Tx go to almost the same positions as the intruders. Moreover, we find that the objective function (3.5), which quantifies the total signal weakness, tends to decrease as time goes on and converges. Note that the minimum value of the objective function (3.5) is not zero due to the altitudes of the intruders.

Next, Figure 3.7 and 3.8 illustrate the simulation results in the case that $N = 3$ and $M = 2$, that is, $N > M$ by the same manner as Figure 3.5 and 3.6. From Figure

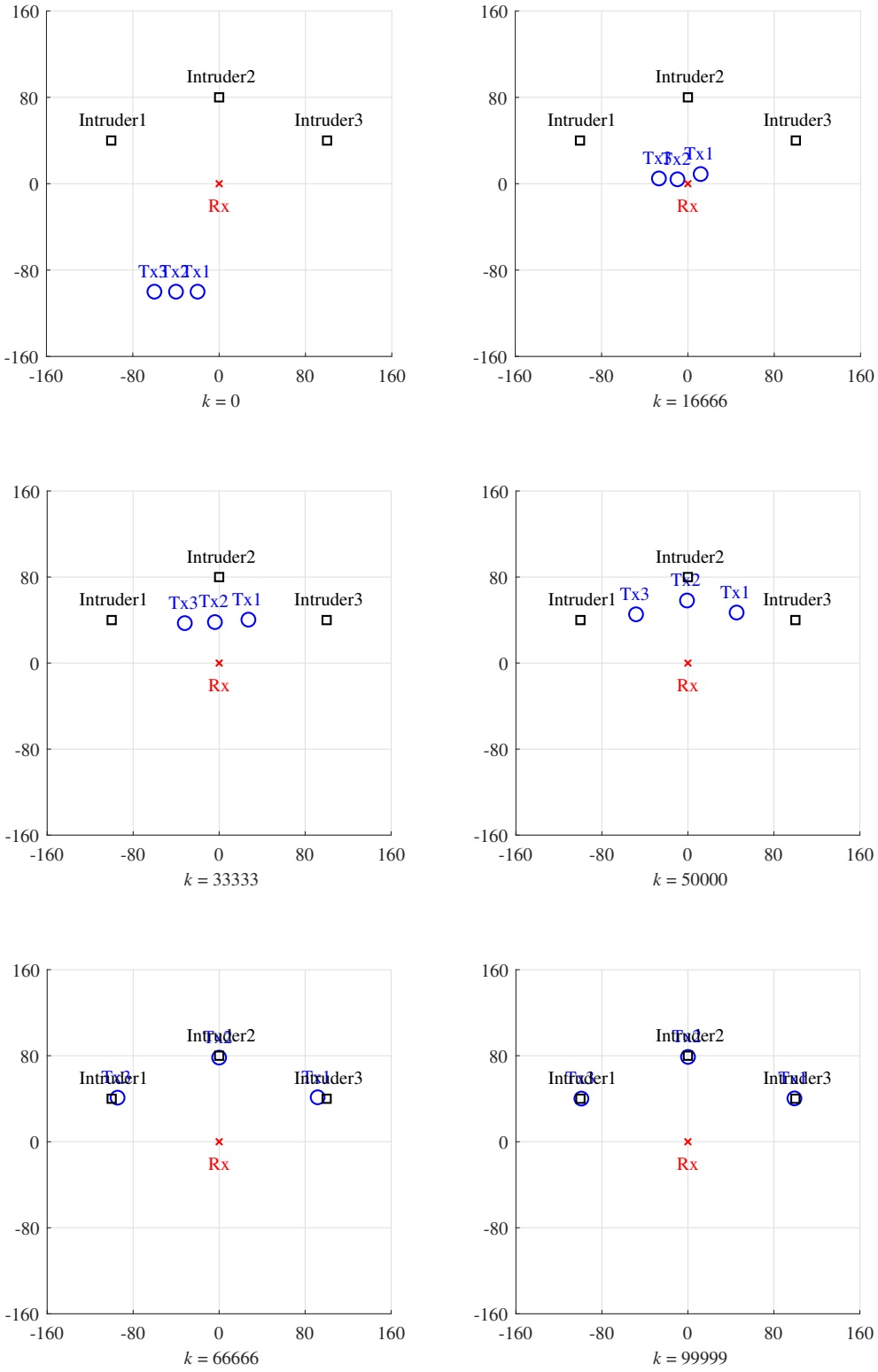

Figure 3.5: Snapshots of Tx, Rx, and intruders for case $\sigma(t) = 1$.

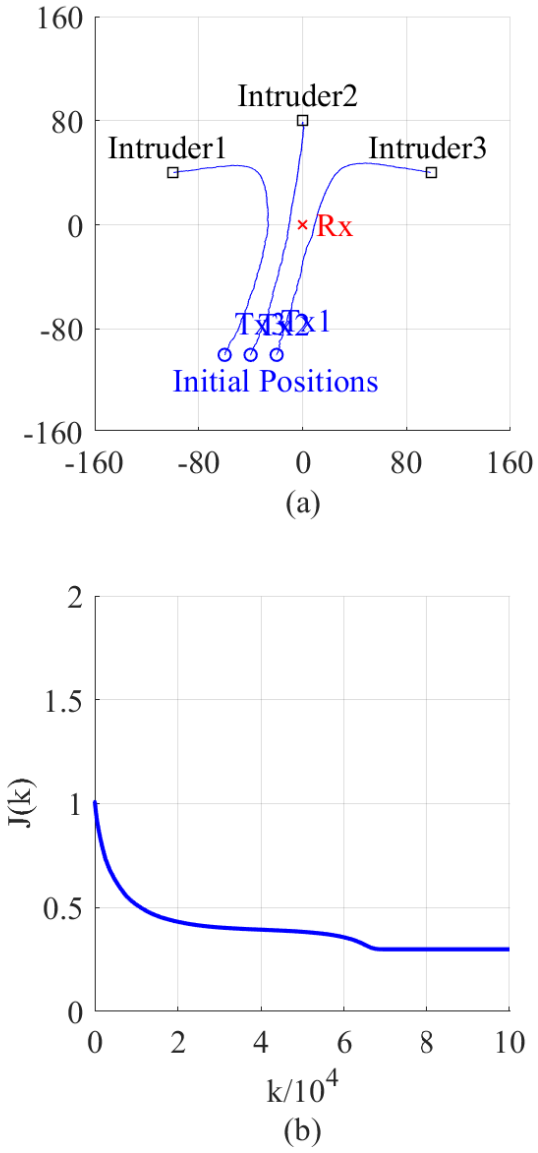

Figure 3.6: Trajectories of Tx and time evolution of $J(x(t))$ for case $\sigma(t) = 1$.

3.7, we can find that the two vehicles' positions converge to the intruders' ones and the other vehicle (Tx2) stops at a location different from the intruders' positions. From Figure 3.8, we see that the positions and the objective function converge.

Then, Figure 3.9 and 3.10 depict the simulation results in the case that $N = 2$ and $M = 3$, that is, $M > N$. From these figures, we can confirm that the vehicles' positions converge to the target locations for maximizing the received signal levels at Rx.

On the other hand, Fig. 3.11 and 3.12 illustrate the simulation result for Case (ii) in the same manner. Furthermore, Fig. 3.13 shows the time series of the angles θ_{ij}. The initial positions of Tx are the same as Case (i). All Tx are approaching nearby the intruders as Case (i) by $k = 16666$ in Fig. 3.11. After that, however, they are moving such that θ_{ij} becomes 180°, i.e., Tx, the intruder, and Rx are lined up in a straight line as illustrated in Fig. 3.11 and Fig. 3.13 without information about the RCS function (3.24). Also, in this case, the objective function (3.5) converges, from which an optimal formation is achieved by the proposed method.

Finally, we give two remarks. First, the performance of the existing methods [26, 27, 30–33] with transmission antennas fixed on the ground corresponds to $J(0)$ in Figures 3.6 and 3.12, which proves that the proposed method has higher performance than the existing methods. Second, the simulation result is expected to be consistent with the real-world performance because

- our method is constructed under the assumption that s_{ij}, which is difficult to model, is almost unknown,
- the control gain $a(k)$ decreases as k goes on, which may prevent from a kind of instability.

3.6 Conclusion

We have proposed a new broadcast control for the radar surveillance system which is composed of the base station and vehicles with the receiving antenna. The proposed

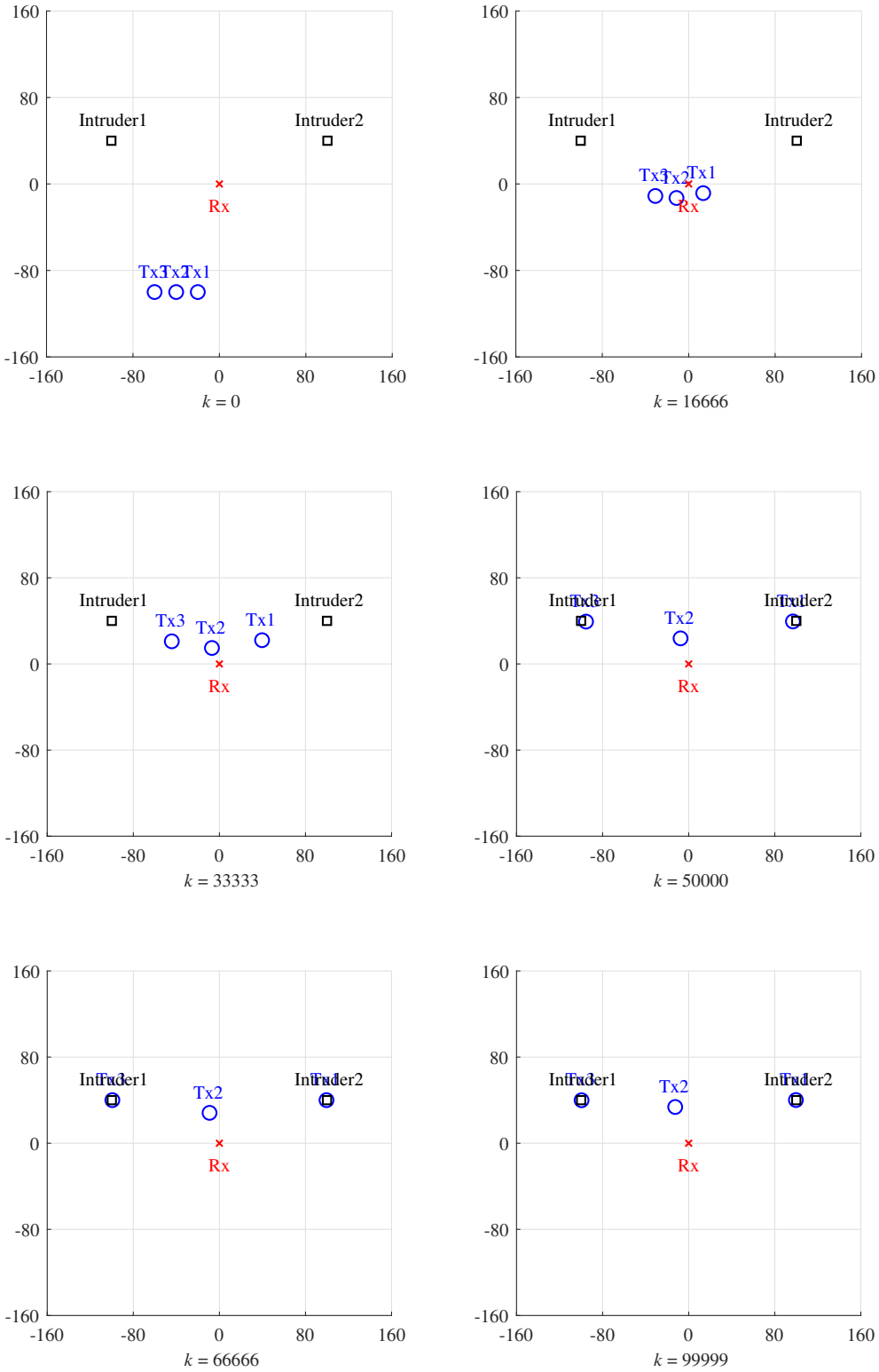

Figure 3.7: Snapshots of Tx, Rx, and intruders for case $\sigma(t) = 1$ and $N > M$.

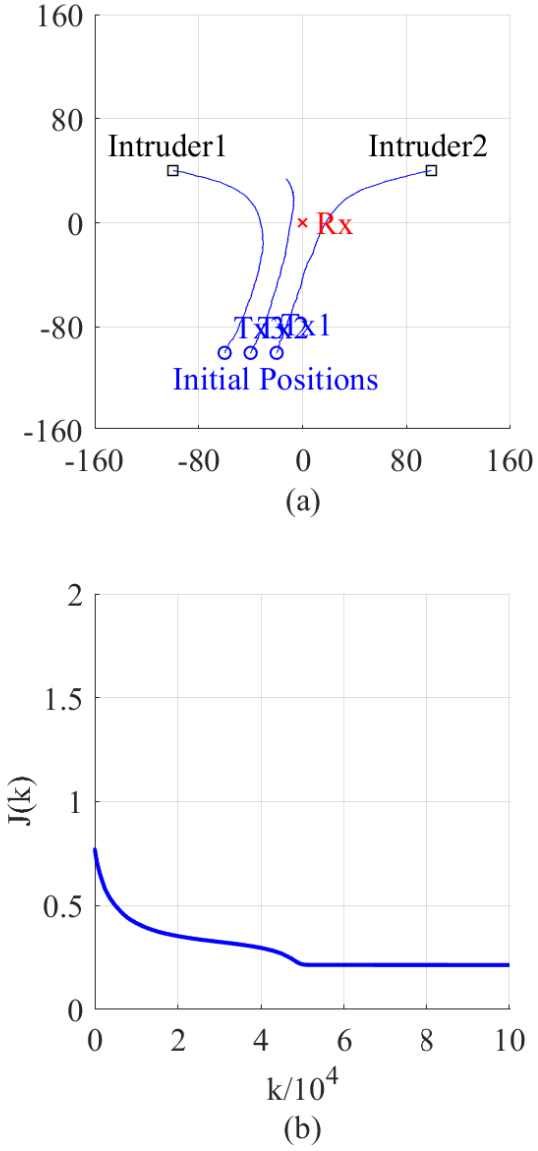

Figure 3.8: Trajectories of Tx and time evolution of $J(x(t))$ for case $\sigma(t) = 1$ and $N > M$.

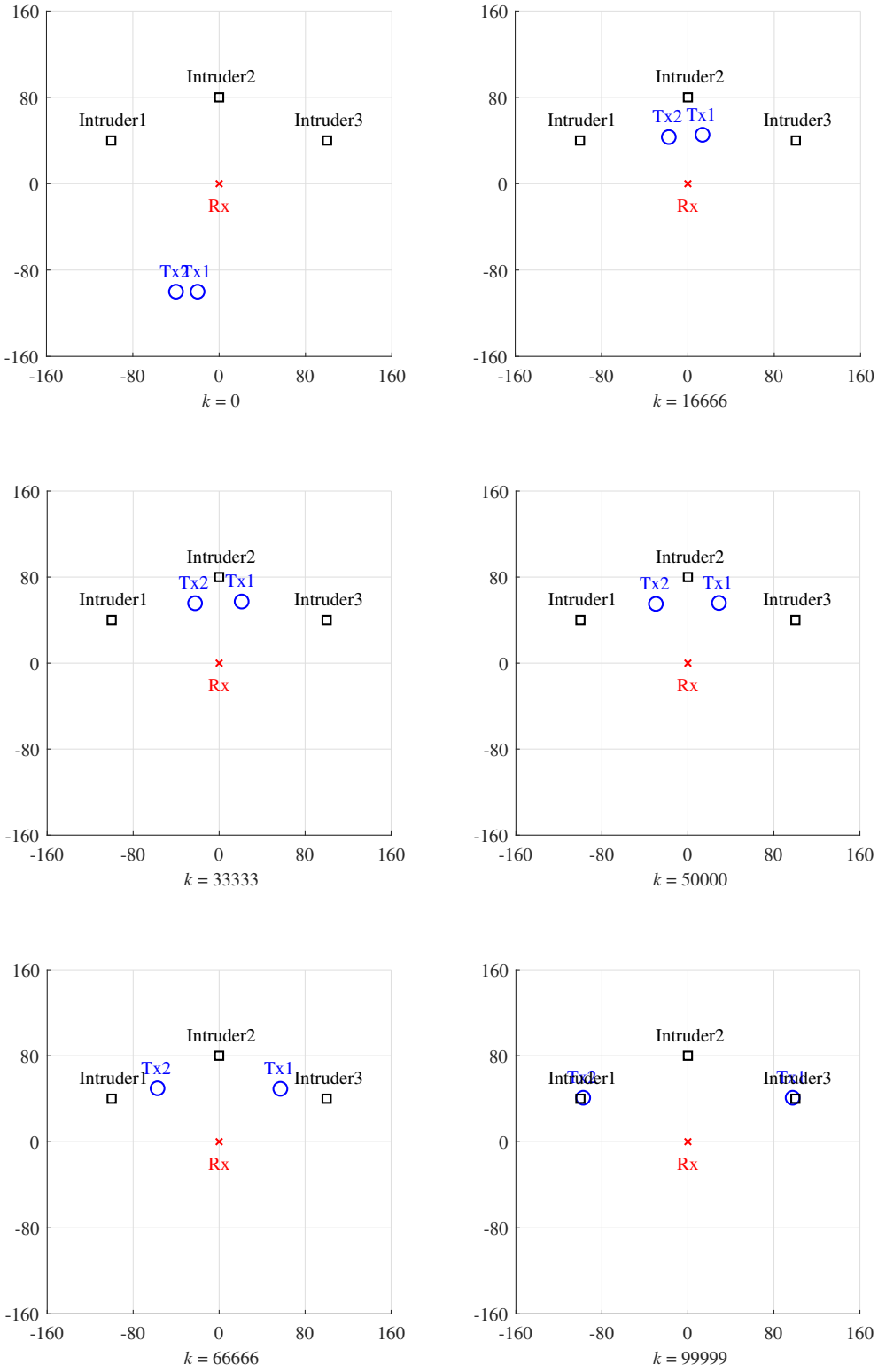

Figure 3.9: Snapshots of Tx, Rx, and intruders for case $\sigma(t) = 1$ and $M > N$.

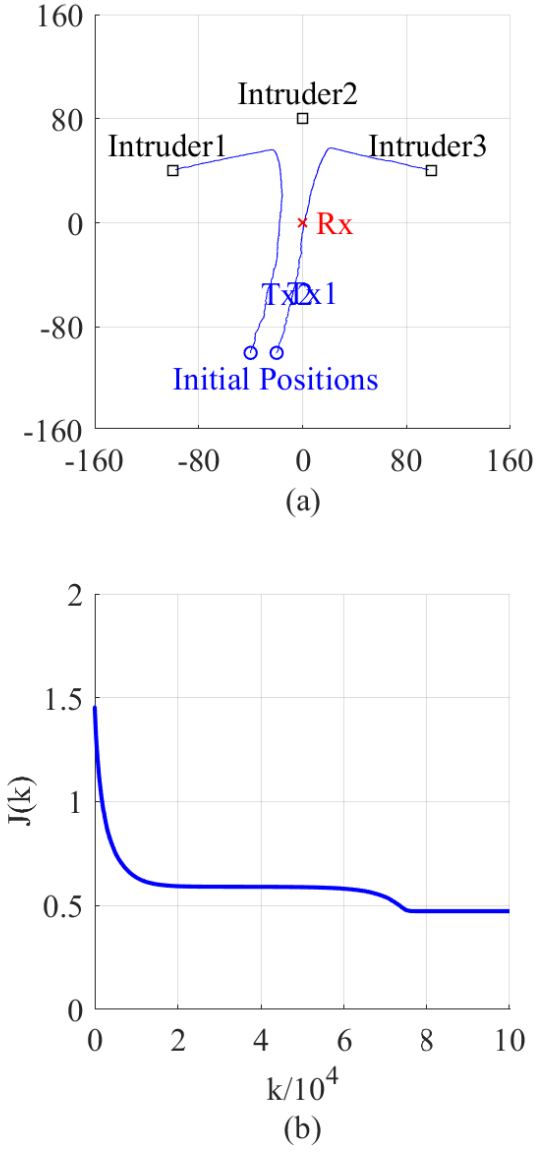

Figure 3.10: Trajectories of Tx and time evolution of $J(x(t))$ for case $\sigma(t) = 1$ and $M > N$.

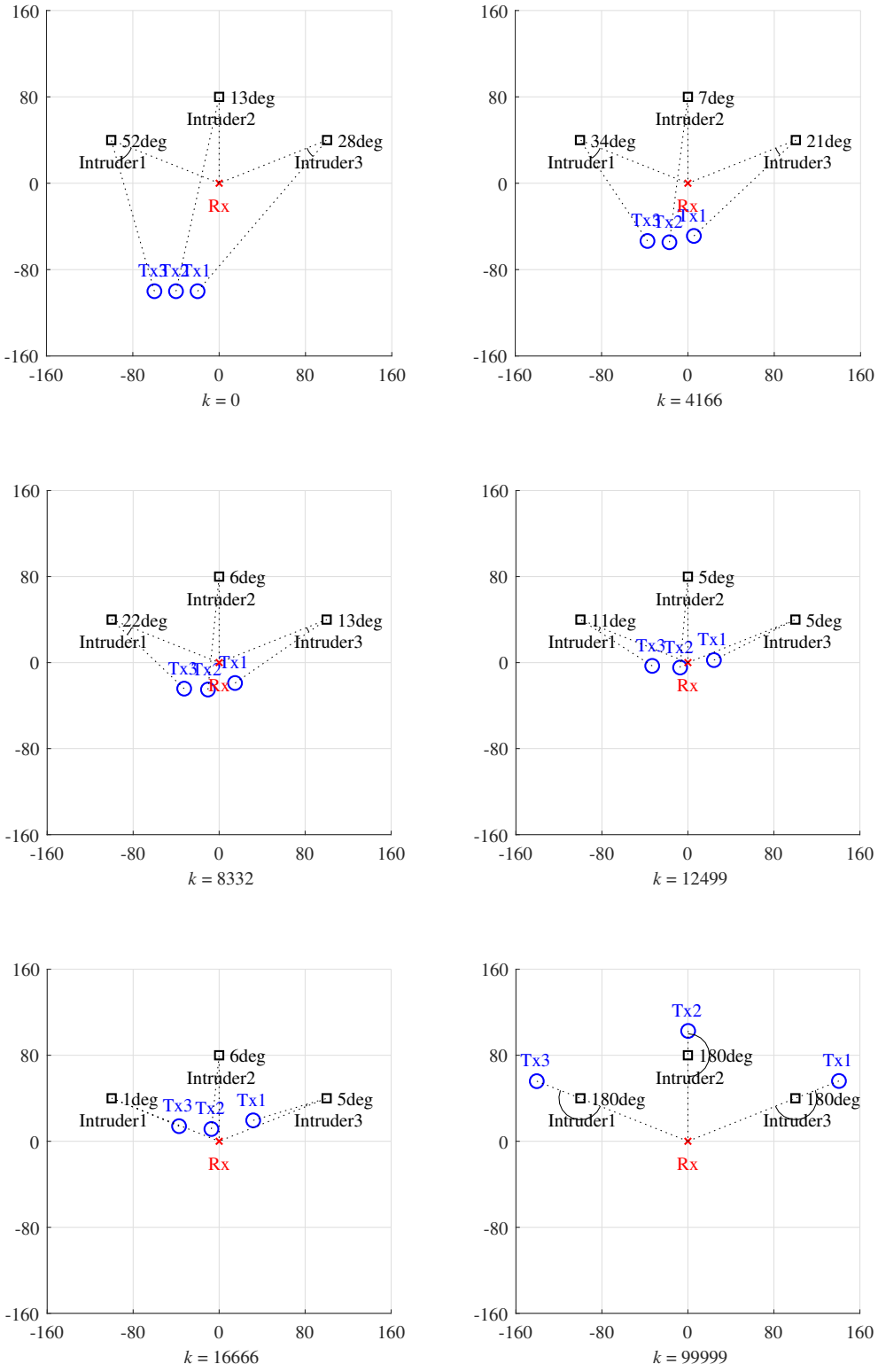

Figure 3.11: Snapshots of Tx, Rx, and intruders for case that radar cross section $\sigma(t)$ is equation (3.24).

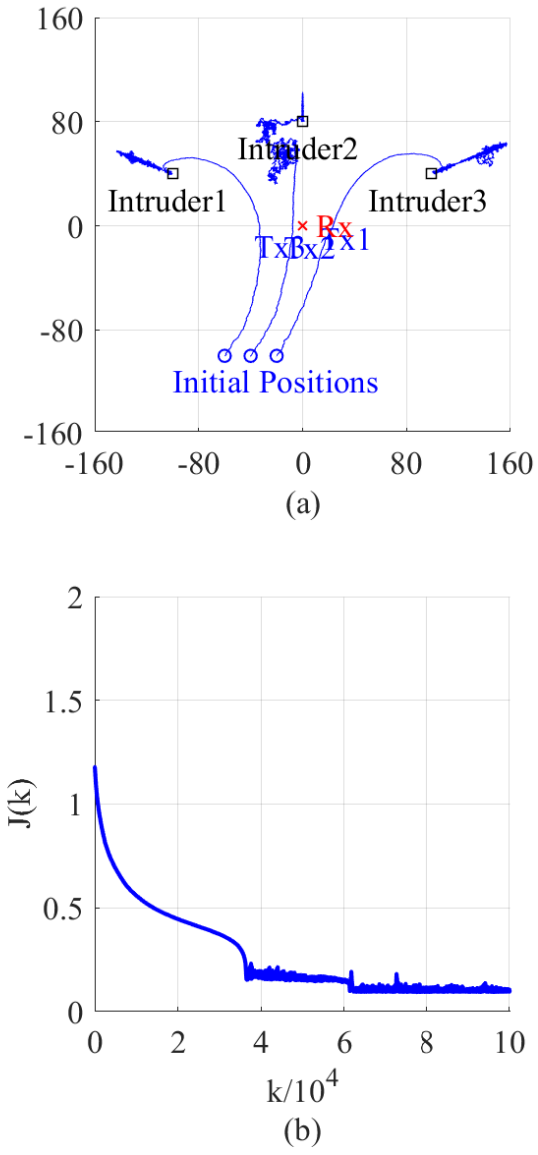

Figure 3.12: Trajectories of Tx and time evolution of $J(x(t))$ for case that $\sigma(t)$ is equation (3.24).

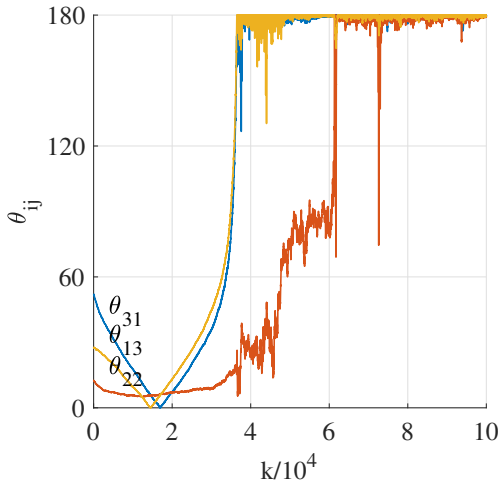

Figure 3.13: Time evolution of angles θ_{ij}.

control algorithm guides the vehicles to a locally optimal formation which maximizes the signal levels received by the base station. Although the locally optimal formation differs depending on the RCS characteristic of the intruders, the vehicles can arrive at the formation shape without using the model of signal transmission. The effectiveness of the proposed control has been verified by the numerical experiments.

Chapter 4

Broadcast Control for Double-integrator Vehicles

4.1 Introduction

We showed the broadcast control for the radar surveillance system in the case that the vehicle dynamics is omni-directional in Chapter 3. However, it was assumed that the dynamics of the vehicle was the single-integrator system with the velocity input. On the other hand, there also exits the vehicle dynamics which is modeled as the multi-integrator system [63,64]. Thus, we also consider the case that the vehicle dynamics is the double-integrator system. In the broadcast control, the equation (2.11) must hold for the convergence. Therefore, the previous works [55,56] about the broadcast control can not be applied to the double integrator because the overall system is different to the equation (2.11) due to the existence of the vehicle velocity as proven in [57]. Thus, we propose the new broadcast control algorithm for the double-integrator system in the chapter [57]. Especially, we propose the four-step switching control law for cancelling the effect of the velocity and satisfying the equation equivalent to (2.11). By utilizing the result of Chapter 3, we can expand the algorithm for position control

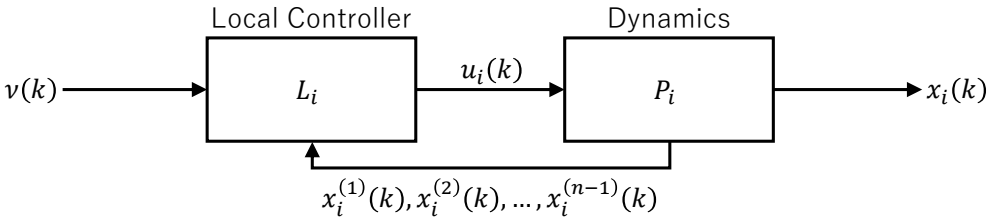

Figure 4.1: Block diagram of vehicle.

to one for signal level maximization.

4.2 Problem Formulation

In the chapter, we consider the vehicle system illustrated in Figure 4.1. In the figure, $x_i^{(j)}(k) \in \mathbb{R}^2$, $j = 1, 2, \ldots, n-1$ is the j th derivative of $x_i(k)$. The states corresponding to the difference of the vehicle position with time such as velocity $x_i^{(1)}(k)$ and acceleration $x_i^{(2)}(k)$ can be measured by the sensor mounted in the vehicle (e.g., Inertial Measurement Unit (IMU)). Although $x_i^{(j)}(k)$, $j = 1, 2, \ldots, n$ includes the measurement error in the real world, we assume that the actual value can be measured for simplicity. On the other hand, the position of the vehicle cannot be measured in the vehicle. In the research, we assume that the dynamics is the double-integrator, that is, $n = 2$.

Let the vehicle dynamics P_i, $i = 1, 2, \ldots, N$ be modeled as

$$P_i : z_i(k+1) = f(z_i(k), u_i(k)), \quad i = 1, 2, \ldots, N \tag{4.1}$$

where

$$z_i(k) = \begin{bmatrix} x_i(k) \\ x_i^{(1)}(k) \end{bmatrix}, \tag{4.2}$$

the function f means the discrete time double-integrator, and

$$f(z_i(k), u_i(k)) = \begin{bmatrix} I_2 & \tau I_2 \\ 0_{2\times 2} & I_2 \end{bmatrix} z_i(k) + \begin{bmatrix} \frac{1}{2}\tau^2 I_2 \\ \tau I_2 \end{bmatrix} u_i(k), \quad i = 1, 2, \ldots, N \tag{4.3}$$

and $\tau \in \mathbb{R}_+$ is the sampling period. In the model, we can regard the control input $u_i(k)$ as the acceleration of the vehicle. The equations (4.1) and (4.3) are derived by ZOH for the continuous double-integrator system with τ.

The local controller L_i, $i = 1, 2, \ldots, N$ outputs the control input $u_i(k)$ as

$$L_i : u_i(k) = h(\nu(k), \nu(k-1), \ldots, \nu(0), \hat{x}_i(k)), \quad i = 1, 2, \ldots, N. \tag{4.4}$$

Additionally, for the description of the overall system, we introduce the symbol $x^{(j)} \in \mathbb{R}^{2N}$ as

$$x^{(j)} = \begin{bmatrix} x_1^{(j)} \\ x_2^{(j)} \\ \vdots \\ x_N^{(j)} \end{bmatrix}. \tag{4.5}$$

The global controller is the same as the conventional one (2.4).

Problem 4.1. We consider the system composed of the equations (4.1), (4.4), and (2.4). We assume that all vehicles stop at the initial time, that is, $x_i^{(1)}(0) = 0$, $i = 1, 2, \ldots, N$. For the system, when any objective function $J : \mathbb{R}^{2N} \to \mathbb{R}_{0+}$ is given, derive the function of the local controller h which satisfies that

$$\lim_{k \to \infty} J(x(k)) = \min_{x \in \mathbb{R}^{2N}} J(x), \tag{4.6}$$

$$\lim_{k \to \infty} x^{(1)}(k) = 0. \tag{4.7}$$

The equation (4.3) can be rewritten as

$$P_i : \begin{cases} x_i(k+1) & = x_i(k) + \tau x_i^{(1)}(k) + \frac{\tau^2}{2} u_i(k), \\ x_i^{(1)}(k+1) & = x_i^{(1)}(k) + \tau u_i(k) \end{cases} \tag{4.8}$$

and the overall system is modeled as

$$P : \begin{cases} x(k+1) & = x(k) + \tau x^{(1)}(k) + \frac{\tau^2}{2} u(k), \\ x^{(1)}(k+1) & = x^{(1)}(k) + \tau u(k). \end{cases} \tag{4.9}$$

4.3 Ineffectiveness of Two-step Broadcast Control

4.3.1 Algorithm

In the section, we explain the two-step broadcast control approach same as the conventional algorithm (2.6), and show the problem 4.1 can not be solved by the approach.

We derive the two-step local controller

$$u(k) = \begin{cases} \bar{u}_{\mathrm{e}}(k), & \text{if } k \text{ is even,} \\ \\ \bar{u}_{\mathrm{o}}(k), & \text{if } k \text{ is odd} \end{cases} \tag{4.10}$$

satisfying with the differential equation same as (2.11) for the system (4.9), where $\bar{u}_{\mathrm{e}}(k) \in \mathbb{R}^{2N}$ and $\bar{u}_{\mathrm{o}}(k) \in \mathbb{R}^{2N}$ mean the control inputs of all vehicles for the case that k is even and odd ($k = 0, 2, 4, \dots$ and $k = 1, 3, 5, \dots$), respectively.

In the former case, the equation same as (2.10) should hold for the system (4.9). Thus, we have

$$c(k)\Delta(k) = \tau x^{(1)}(k) + \frac{\tau^2}{2}\bar{u}_{\mathrm{e}}(k), \quad k = 0, 2, 4, \dots, \tag{4.11}$$

that is,

$$\bar{u}_{\mathrm{e}}(k) = \frac{2}{\tau^2}c(k)\Delta(k) - \frac{2}{\tau}x^{(1)}(k). \tag{4.12}$$

Next, from the equation (4.9), the state transition from k to $k+2$ is given by

$$\begin{cases} x(k+2) = x(k) + 2\tau x^{(1)}(k) + \frac{3\tau^2}{2}u(k) + \frac{\tau^2}{2}u(k+1), \\ \\ x^{(1)}(k+2) = x^{(1)}(k) + \tau u(k) + \tau u(k+1). \end{cases} \tag{4.13}$$

By substituting the equation (4.12) into $u(k)$ in the equation (4.13), we have

$$x(k+2) = x(k) + 3c(k)\Delta(k) - \tau x^{(1)}(k) + \frac{\tau^2}{2}\bar{u}_{\mathrm{o}}(k+1), \quad k = 0, 2, 4, \dots. \tag{4.14}$$

The equation should correspond with the differential equation (2.11), then

$$-a(k)d(k, k+1) = 3c(k)\Delta(k) - \tau x^{(1)}(k) + \frac{\tau^2}{2}\bar{u}_{\mathrm{o}}(k+1), \quad k = 0, 2, 4, \dots. \tag{4.15}$$

Therefore, the control input in the case $k = 1, 3, 5, \dots$ is given by

$$\bar{u}_{\mathrm{o}}(k) = -\frac{6}{\tau^2}c(k-1)\Delta(k-1) - \frac{2}{\tau^2}a(k-1)d(k-1, k) + \frac{2}{\tau}x^{(1)}(k-1). \tag{4.16}$$

4.3.2 Convergence Analysis

However, we prove that Problem 4.1 can not be solved by the two-step local controller (4.10), (4.12), and (4.16).

Lemma 4.1. We consider the system composed of the equations (4.3), (4.10), (4.12), (4.16), and (2.4). We assume that the objective function J is differentiable and has some local optimums and there exists $x^* \in \mathbb{R}^{2N}$ satisfying with $\nabla J(x^*) = 0_{2N\times 1}$. Furthermore, we also assume that J satisfies the condition (B1), $a(k)$ and $c(k)$ in (4.12) and (4.16) satisfy the condition (B3), and $\Delta(k)$ satisfies the condition (B4) in Lemma 2.1. Then, there exists an objective function J such that

$$\lim_{k\to\infty} x^{(1)}(k) \neq 0. \tag{4.17}$$

Proof. From the equations (4.3), (4.10), and $x^{(1)}(0) = 0$, the velocity at $k = 0, 2, 4, \ldots$ can be written as

$$x^{(1)}(k) = -\frac{2}{\tau} \sum_{l\in\{0,2,\ldots,k-2\}} a(l)d(l, l+1) - \frac{2}{\tau} \sum_{l\in\{0,2,\ldots,k-2\}} c(l)\Delta(l). \tag{4.18}$$

Next, from the equation (2.11), we have

$$\sum_{l\in\{0,2,\ldots,k-2\}} a(l)d(l, l+1) = -x(k) + x(0). \tag{4.19}$$

By substituting the equation into (4.18), we have

$$x^{(1)}(k) = \frac{2}{\tau}\left(x(k) - x(0)\right) - \frac{2}{\tau} \sum_{l\in\{0,2,\ldots,k-2\}} c(l)\Delta(l). \tag{4.20}$$

In the equation (4.20), the position time series $x(0), x(2), x(4), \ldots$, converges to x^* since the equation (2.11) holds by the local controller (4.10). Thus, velocity time series $x^{(1)}(0), x^{(1)}(2), x^{(1)}(4), \ldots$ converges to

$$x_{\mathrm{e}}^{*(1)} = \frac{2}{\tau}\left(x^* - x(0)\right) - \frac{2}{\tau}\delta, \tag{4.21}$$

$$\delta = c(0)\Delta(0) + c(2)\Delta(2) + c(4)\Delta(4) + \cdots. \tag{4.22}$$

Note that $\delta < \infty$ holds from the conditions (B3) and (B4) in Lemma 2.1.

On the other hand, from the equations (4.3) and (4.10), and (4.12), we have

$$x^{(1)}(k+1) = -x^{(1)}(k) + \frac{2}{\tau}c(k)\Delta(k). \tag{4.23}$$

Then, from the conditions (B3) and (B4), the time series $x^{(1)}(1), x^{(1)}(3), x^{(1)}(5), \ldots$ converges to

$$x_{\mathrm{o}}^{*(1)} = -x_{\mathrm{e}}^{*(1)}. \tag{4.24}$$

For the objective function J with x^* satisfying

$$x^* \neq x(0) + \delta, \tag{4.25}$$

from the equations (4.21) and (4.24), we have

$$x_{\mathrm{e}}^{*(1)} \neq 0, \quad x_{\mathrm{o}}^{*(1)} \neq 0 \tag{4.26}$$

and

$$\lim_{k\to\infty} x^{(1)}(k) \neq 0. \tag{4.27}$$

□

Note that from the equation (4.25), Problem 4.1 can be solved only if the following special condition about the reference formation holds:

$$x^* = x(0) + \delta. \tag{4.28}$$

We can find the condition rarely holds.

4.3.3 Numerical Simulation

We show the numerical simulation results for evaluating our claim in Lemma 4.1. We set the same conditions as the case of simulation with the conventional local controller in Section 2.5.1. Additionally, the sampling period is given by $\tau = 10^{-1}$.

Figure 4.2 and 4.3 illustrate the simulation result. These figures are illustrated in the same manner as Figure 2.4 and 2.5.

From Figure 4.2, we can find that vehicle positions converge to the reference formation at $k = 4000$ and equilibrate at the same place after that. Additionally, from Figure 4.3, we see that the objective function converges to 0 and positions converge to 6 or -6 at $k = 5000$. These results are the same as Figure 2.4 and correspond to the equation (4.6).

However, from the result of the velocity time series illustrated at the bottom of Figure 4.3, we can confirm that the velocities do not converge and vibrate as the equation (4.24) in Lemma 4.1.

From these results, we can say that the two-step local controller composed of (4.10), (4.12), and (4.16) is not a solution for Problem 4.1.

4.4 Proposed Four-step Broadcast Control

4.4.1 Algorithm

In Section 4.3 and 4.3.3, we showed the ineffectiveness of the two-step local controller. Thus, we derive the proposed local controller for solving Problem 4.1. It is the weak point of the two-step local controller (4.10), (4.12), and (4.16) that the vehicles' velocities are not explicitly considered and controlled.

Therefore, we develop the local controller by which not only positions but also velocities are controlled. So, we propose to introduce additional time for controlling the velocities. Figure 4.4 and 4.5 illustrate the switching timing of the conventional two-step local controller and the proposed four-step one. By the proposed switching timing shown in Figure 4.5, the following transitions are realized in $k = 0, 4, 8, \ldots$:

$$\begin{cases} x(k+2) = x(k) + c(k)\Delta(k), & \text{(4.29a)} \\ x(k+4) = x(k+2) - c(k)\Delta(k) - a(k)d(k, k+2). & \text{(4.29b)} \end{cases}$$

Thus, we derive the local controller satisfying that the total displacement from k to $k+2$ is equal to $c(k)\Delta(k)$. We can find that the number of unknown parameters (the elements of $u(k)$ and $u(k+1)$) is $4N$, whereas the number of equations (the degree of

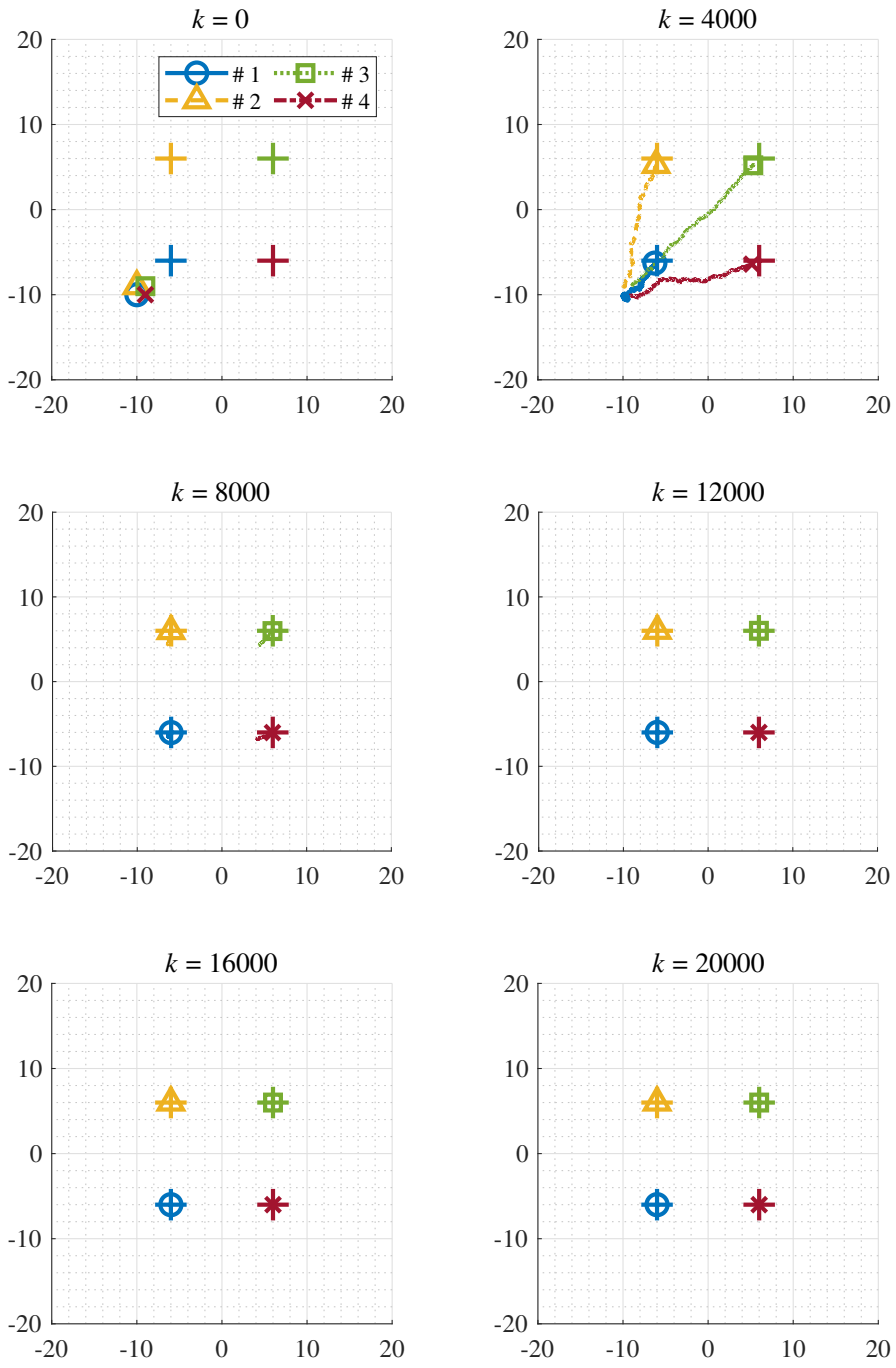

Figure 4.2: Positions transition of vehicles with double-integrator dynamics and two-step local controller in two-dimensional plane for objective function (2.20).

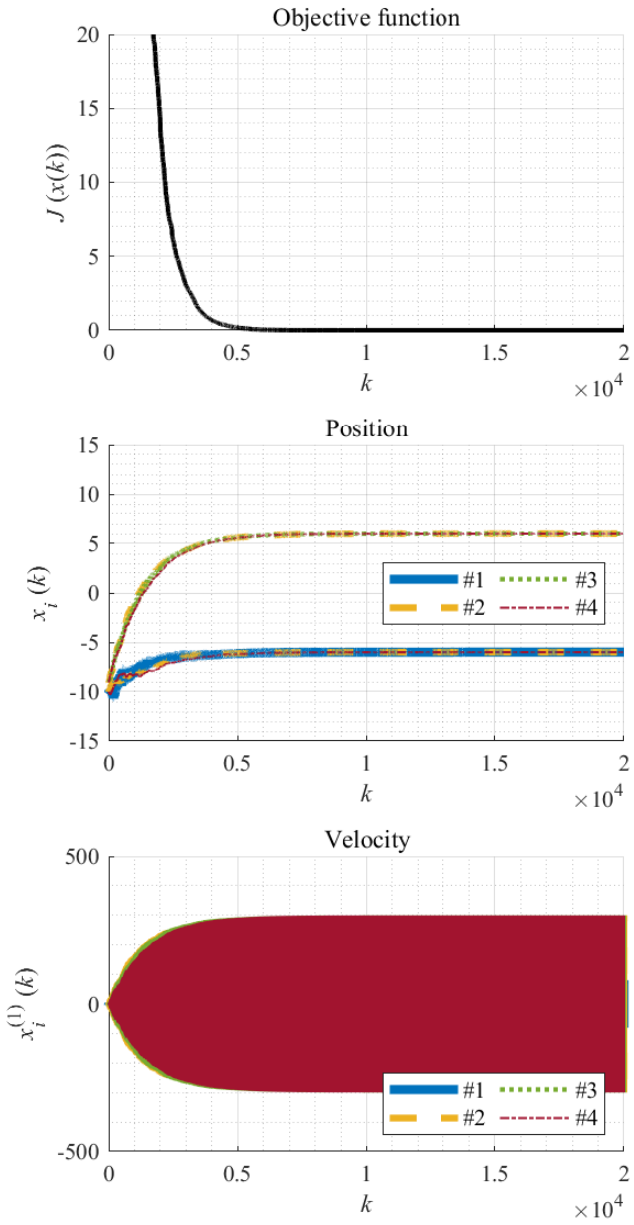

Figure 4.3: Time series of the objective function (2.20), vehicles positions, and velocities by two-step local controller.

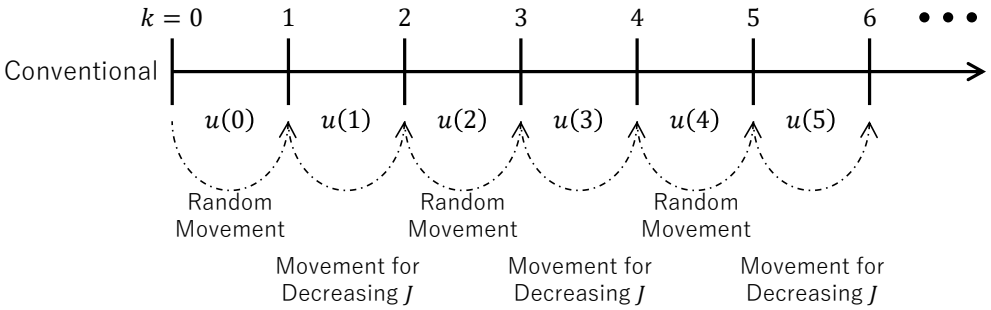

Figure 4.4: Switching timing of conventional broadcast control.

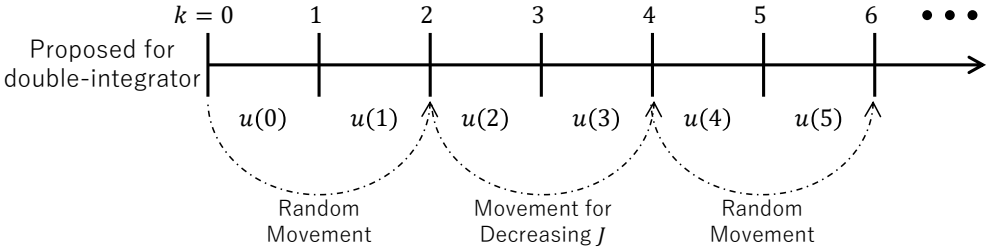

Figure 4.5: Switching timing of proposed four-step broadcast control.

$c(k)\Delta(k))$ is $2N$, which means the degree of freedom for $u(k)$ and $u(k+1)$ emerges. Then, we develop the local controller L_i, $i = 1, 2, \ldots, N$ by which $x^{(1)}(k+2) = 0_{2N\times 1}$ in the timing from k to $k+2$. On the other hand, about the timing from $k+2$ to $k+4$, we develop the local controller in the same manner as the case of the timing from k to $k+2$, that is, we develop the local controller by which the total displacement is equal to $-c(k)\Delta(k) - a(k)d(k, k+2)$ and $x^{(1)}(k+4) = 0_{2N\times 1}$.

We propose the function of the local controller h in the equation (4.4) as

$$h(\nu(k), \nu(k-1), \ldots, \nu(0), \hat{x}_i(k)) = \begin{cases} \frac{c(k)}{\tau^2}\Delta_i(k) - \frac{2}{\tau}x_i^{(1)}(k) & \text{if } k \in \mathbb{N}_0, \\ u_i^2(\nu(k), \nu(k-2), x_i^{(1)}(k)) & \text{if } k \in \mathbb{N}_2, \\ -u_i(k-1) & \text{if } k \in \mathbb{N}_{13}, \end{cases} \quad (4.30)$$

where

$$u_i^2(\nu(k), \nu(k-2), x_i^{(1)}(k)) = -\frac{c(k-2)}{\tau^2}\Delta_i(k-2) - \frac{2}{\tau}x_i^{(1)}(k) - \frac{a(k-2)}{\tau^2}\frac{\nu(k)-\nu(k-2)}{c(k-2)}\Delta_i^{-1}(k-2) \quad (4.31)$$

and $\mathbb{N}_0 = \{0, 4, 8, \ldots, \}$, $\mathbb{N}_2 = \{2, 6, 10, \ldots, \}$, $\mathbb{N}_{13} = \{1, 3, 5, \ldots, \}$.

4.4.2 Convergence Analysis

We prove the convergence of the proposed four-step local controller (4.4) and (4.30).

Theorem 4.1. We consider the system composed of the equations (4.3), (4.4), and, (2.4). When the function of the local controller h is given by the equation (4.30), the equation (4.29) holds. Additionally, we assume that the objective function J is differentiable and there exits $x^* \in \mathbb{R}^{2N}$ satisfying $\nabla J(x^*) = 0_{2N\times 1}$. When the conditions (B1), (B3), and (B4) hold for J, $a(k)$, and $c(k)$ and the following other conditions

(B2') x^* is asymptotically stable equilibrium of the gradient system $\dot{\eta}(t) = -\nabla J(\eta(t))$ in the Lyapunov sense,

(B5') $E[J(x(k) + c(k)\Delta(k))^2]$ is bounded for all $k \in \mathbb{N}_0$,

(B6') For a compact set $\mathbb{S} \subseteq \mathbb{R}^{2N}$ such that $\dot{\eta}(t) = -\nabla J(\eta(t))$ with $x(0) \in \mathbb{S}$ results in $\lim_{k\to\infty} x(\infty) = x^*$, $x(k) \in \mathbb{S}$ occurs infinitely often for almost all sample points of $\Delta_i(k)$ $(i = 1, 2, \ldots, N,\ k = 0, 1, \ldots)$,

(B7') $\sup_{k\in\mathbb{N}_0} \|x(k)\| < \infty$, w.p.1.,

hold,

$$\lim_{k\to\infty} x(k) = x^*, \quad \text{w.p.1}, \tag{4.32}$$

$$\lim_{k\to\infty} x^{(1)}(k) = 0. \tag{4.33}$$

Proof. By replacing k with $k+2$ in the equation (4.13), we have

$$\begin{cases} x(k+4) = x(k+2) + 2\tau x^{(1)}(k+2) + \frac{3\tau^2}{2}u(k+2) + \frac{\tau^2}{2}u(k+3), \\ x^{(1)}(k+4) = x^{(1)}(k+2) + \tau u(k+2) + \tau u(k+3). \end{cases} \tag{4.34}$$

First, we prove that the equation (4.29) holds. When $k \in \mathbb{N}_0$, from the equations (4.4) and (4.30), we have

$$u(k) = \frac{1}{\tau^2}c(k)\Delta(k) - \frac{2}{\tau}x^{(1)}(k), \tag{4.35}$$

$$u(k+1) = -u(k). \tag{4.36}$$

By substituting the above equations into the equation (4.13), we can find that the equations (4.29a) and

$$x^{(1)}(k+2) = x^{(1)}(k) \tag{4.37}$$

hold. On the other hand, since $k+2 \in \mathbb{N}_2$, from the equations (4.4), (4.30), and (4.31), we have

$$u(k+2) = -\frac{c(k)}{\tau^2}\Delta(k) - \frac{2}{\tau}x^{(1)}(k+2) - \frac{a(k)}{\tau^2}\frac{\nu(k+2)-\nu(k)}{c(k)}\Delta^{-1}(k), \tag{4.38}$$

$$u(k+3) = -u(k+2). \tag{4.39}$$

By substituting the above equations into the equation (4.34), we can also find that the equations (4.29b) and

$$x^{(1)}(k+4) = x^{(1)}(k+2). \tag{4.40}$$

Thus, the equation (4.29) holds. Next, we also prove the latter proposition.

From the equations (4.37), (4.40), and $x^{(1)}(0) = 0_{2N\times 1}$, we have

$$x^{(1)}(0) = x^{(1)}(2) = x^{(1)}(4) = \cdots = 0_{2N\times 1}. \tag{4.41}$$

Then, we consider different three cases about k.

(i) $k \in \mathbb{N}_0$

By substituting the equations (2.4) and (4.29a) into (4.29b), the difference equation from k to $k+4$ can be written as

$$x(k+4) = x(k) - a(k)\frac{J(x(k)+c(k)\Delta(k)) - J(x(k))}{c(k)}\Delta^{(-1)}(k). \tag{4.42}$$

The system corresponds to the equation (2.15) in which $k+1$ is replaced with $k+4$ in Lemma 2.1. Therefore, when the conditions corresponding to (B1) to (B7) in Lemma 2.1, that is, (B1), (B3), (B4), (B2'), (B5'), (B6'), and (B7'), hold, the sequence $x(0), x(4), x(8), \ldots$ converges to x^* with probability 1 from Lemma 2.1.

(ii) $k \in \mathbb{N}_2$

Since $k-2 \in \mathbb{N}_0$ in the case that $k \in \mathbb{N}_2$, from the equation (4.29a),

$$x(k) - x(k-2) = c(k-2)\Delta(k-2) \tag{4.43}$$

holds. Thus, when the conditions (B3) and (B4) hold, the sequence $\|x(2)-x(0)\|,\ \|x(6)-x(4)\|,\ \|x(10)-x(8)\|,\ \ldots$ converges to 0. From the fact and the result of the case (i), the sequence $x(2), x(6), x(10), \ldots$ converges to x^* with probability 1.

(iii) $k \in \mathbb{N}_{13}$

From the equation (4.9),

$$x(k) = x(k-1) + \tau x^{(1)}(k-1) + \frac{\tau^2}{2} u(k-1) \tag{4.44}$$

holds. We confirm convergence about each term on the right side of the above equation.

Since $k-1 \in \mathbb{N}_0$ or $k-1 \in \mathbb{N}_2$, from the result of the case (i) and (ii), $x(k-1)$ converges to x^* with probability 1. About the second term, from the equation (4.41), $x^{(1)}(k-1) = 0_{2N\times 1}$. From the equations (4.30) and (4.31), we have

$$u(k-1) = \frac{c(k-1)}{\tau^2}\Delta_i(k-1) - \frac{2}{\tau}x_i^{(1)}(k-1), \quad k-1 \in \mathbb{N}_0 \tag{4.45}$$

and

$$\begin{aligned} u(k-1) &= -\frac{c(k-3)}{\tau^2}\Delta_i(k-3) - \frac{2}{\tau}x_i^{(1)}(k-1) \\ &\quad -\frac{a(k-3)}{\tau^2}\frac{\nu(k-1)-\nu(k-3)}{c(k-3)}\Delta_i^{-1}(k-3), \quad k-1 \in \mathbb{N}_2. \end{aligned} \tag{4.46}$$

Thus, when the conditions (B3) and (B4) hold, from the equation (4.41), $u(k-1)$ converges to $0_{2N\times 1}$. From these facts and the equation (4.44), the sequence $x(1), x(3), x(5), \ldots$ converges to x^* with probability 1.

On the other hand, about the velocity, from the equation (4.9),

$$x^{(1)}(k) = x^{(1)}(k-1) + \tau u(k-1) \tag{4.47}$$

holds. From the equation (4.41) and the fact that $u(k-1)$ converges to $0_{2N\times 1}$, $x^{(1)}(k)$ also converges to $0_{2N\times 1}$.

From the equation (4.41) and the cases (i), (ii), and (iii), the equation (4.32) and (4.33) hold. □

4.4.3 Numerical Simulation

We show the numerical simulation results for evaluating the effectiveness of our proposed algorithm (4.30) and the results of the convergence analysis in Theorem 4.1. We set the same conditions in Section 2.5.1, 2.5.2 and 4.3.3.

Formation Control

Figure 4.6 and 4.7 illustrate the simulation result for the objective function of formation control (2.20). These figures are illustrated in the same manners as Figure 2.4 and 2.5.

From Figure 4.6, we see that the vehicles' positions converge to the reference formation like Figure 2.4 and 4.2. On the other hand, in Figure 4.7, the time series of the vehicles' velocities converge as well as the objective function and the vehicles' positions unlike Figure 4.3. From these results, we can confirm that both positions and velocities can be controlled and the effectiveness of the proposed four-step local controller (4.30). However, we also see that the elapsed time for convergence in Figure 4.7 is twice as the case in Figure 2.5 due to increasing the number of steps in the local controller.

Coverage Control

Figure 4.8 and 4.9 illustrate the simulation result for the objective function corresponding to coverage control (2.22). These figures are illustrated in the same manners as Figure 2.7 and 2.8.

From Figure 4.8, we see that the four vehicles converge to the positions for which the areas of Voronoi regions are almost equal in the bounded area like Figure 2.7. From Figure 4.9, we can find that the time series of the vehicles' velocities converge to 0 like Figure 4.6. From these results, we can find that the proposed four-step local controller is also effective for the objective function (2.22). The elapsed time for convergence is also twice as the case in Figure 2.8 like Section 4.4.3.

Radar Surveillance System

Finally, we show the simulation results for the case that the vehicle dynamics is the double-integrator system in the radar surveillance system in Capter 3. In this case, the objective function is the equations (3.4) and (3.10) and the local controller is given by (4.4) and (4.30). The parameters are almost same as Section 3.5 and $a_0 = 2.0 \times 10$ and $c_0 = 1.0 \times 10^{-4}$. Figure 4.10 and 4.11 show the result by the same manner of Figure 3.5 and 3.6. We can find that the almost same result is obtained as in the case of Figure 3.5 and 3.6. Additionally, from Figure 4.11, the velocities of the vehicles also converge.

4.5 Conclusion

In the chapter, we have proposed a new broadcast control algorithm for the vehicle with the dynamics of the double-integrator system. In the double-integrator system, the control input affects not only the vehicle position but also the velocity. Nevertheless, we have shown that the local minimization is achieved for the objective function by the proposed control. The effectiveness of the proposed control has been verified by the numerical simulations. In the future, we will expand the control law to the case of the multi-integrator system. Additionally, for realizing the proposed algorithm, the velocity sensor or the so-called "soft-sensor" such as observer in the control literature is needed, which has the measurement or estimation error and results in the increasing complexity of the control system. Therefore, we will also study the simple broadcast control algorithm for the system with such noise.

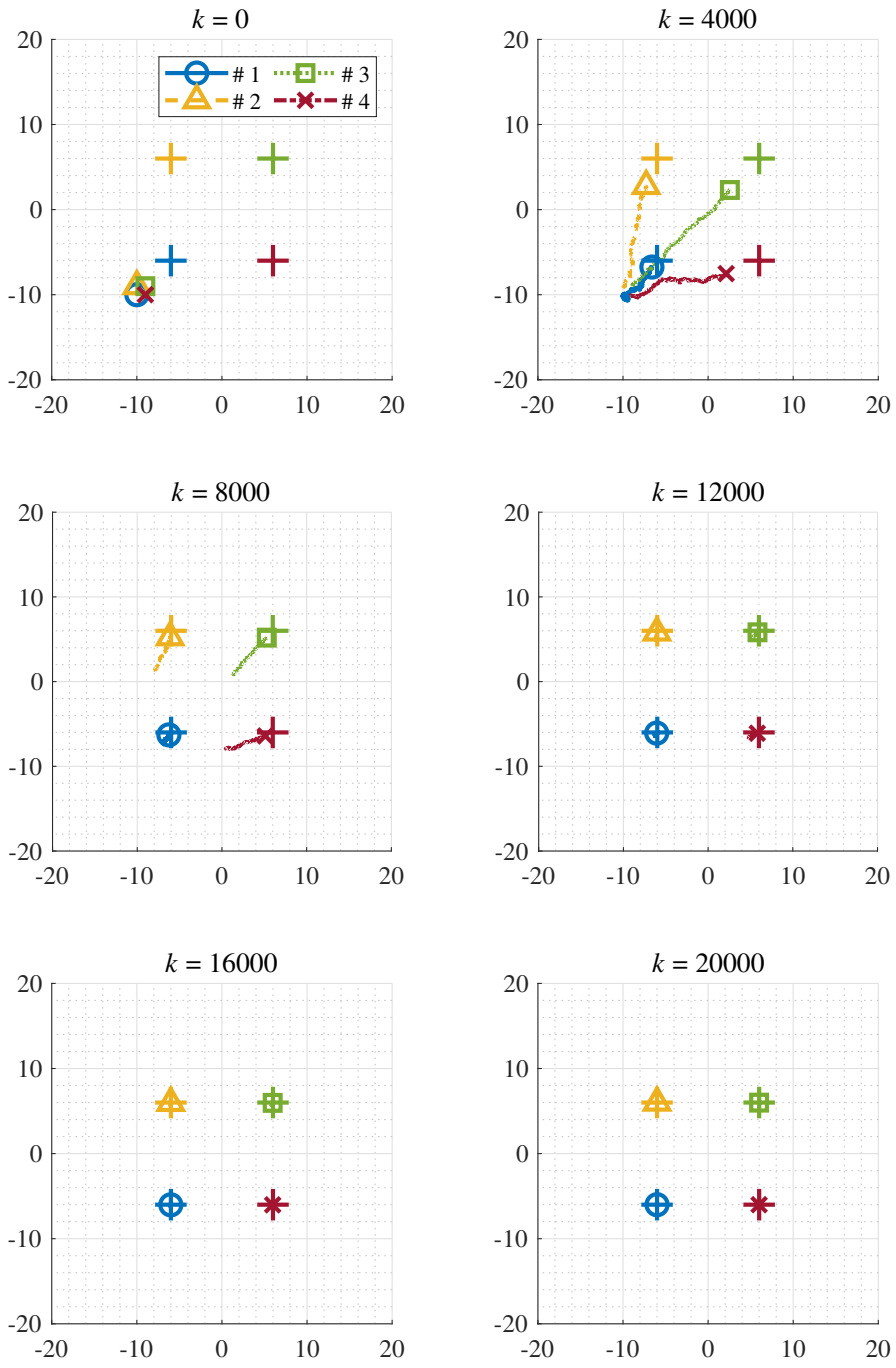

Figure 4.6: Positions transition of vehicles with double-integrator dynamics and four-step local controller in two-dimensional plane for objective function (2.20).

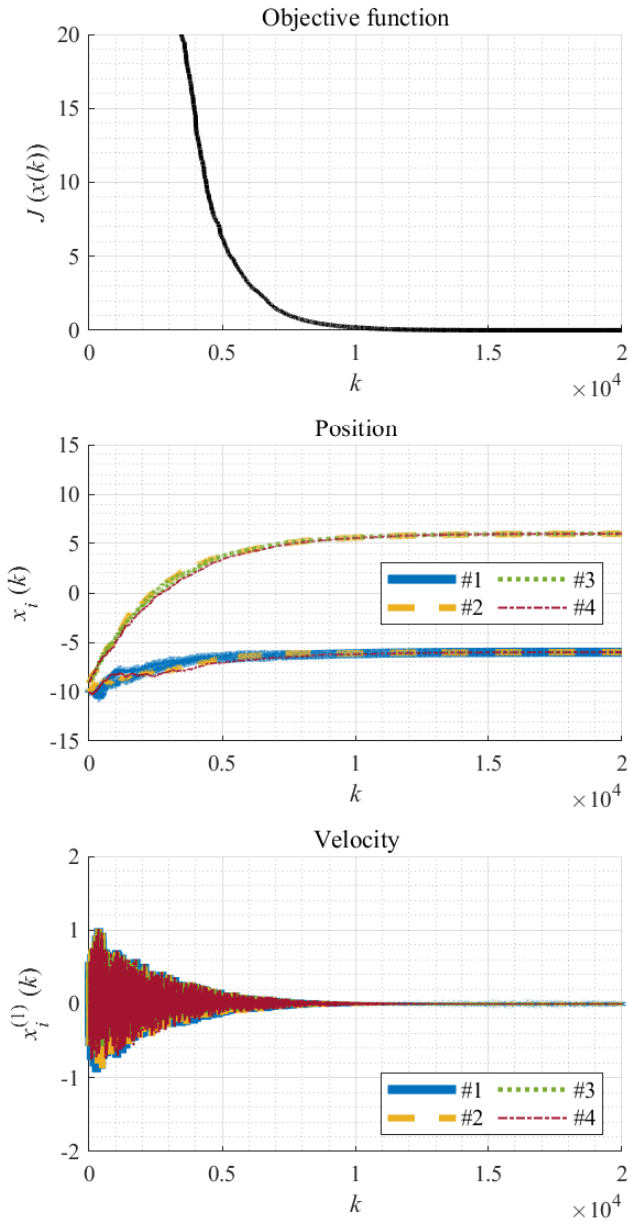

Figure 4.7: Time series of objective function (2.20), vehicles positions, and velocities by four-step local controller.

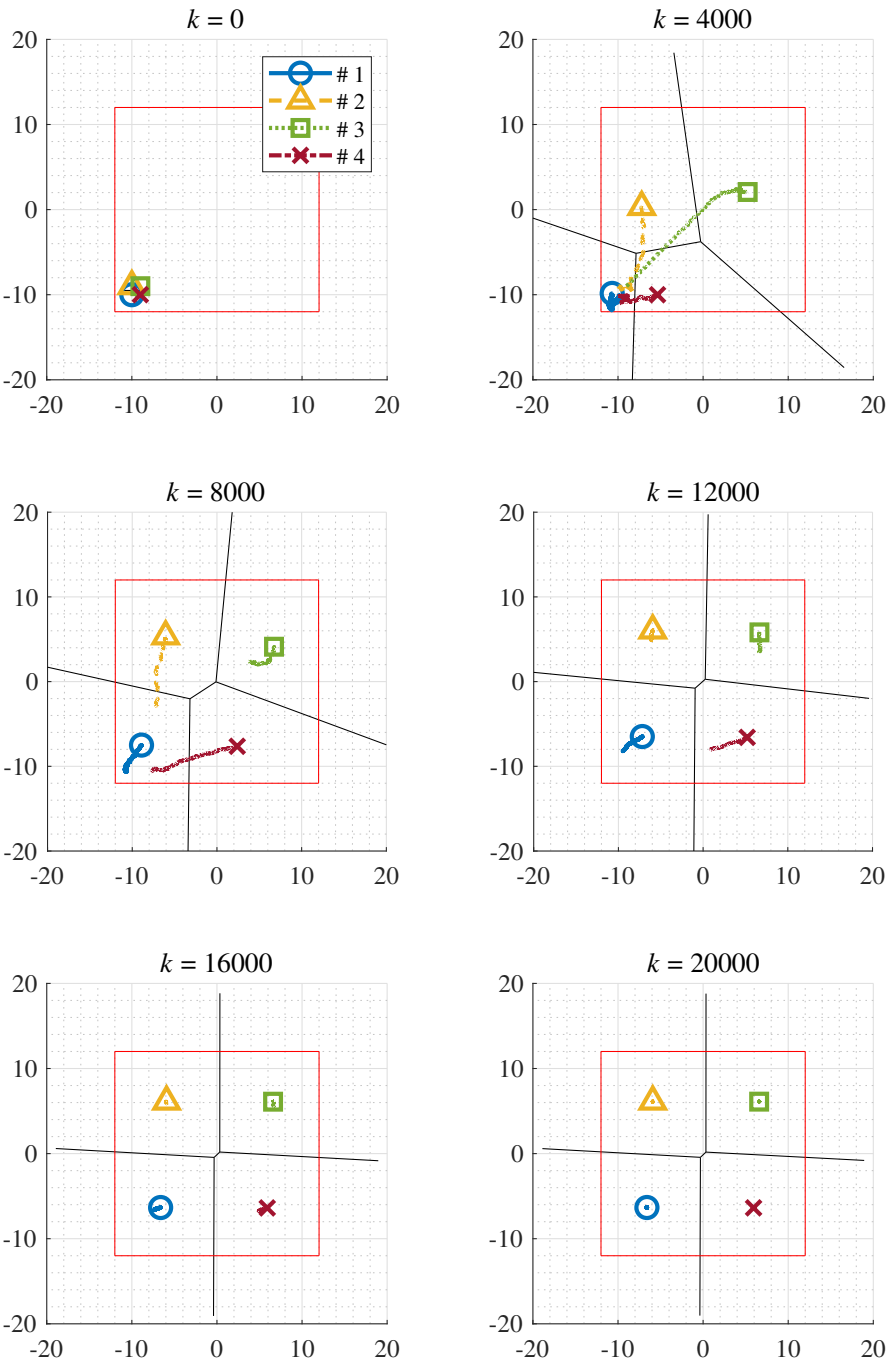

Figure 4.8: Positions transition of vehicles with double-integrator dynamics and four-step local controller in two-dimensional plane for objective function (2.22).

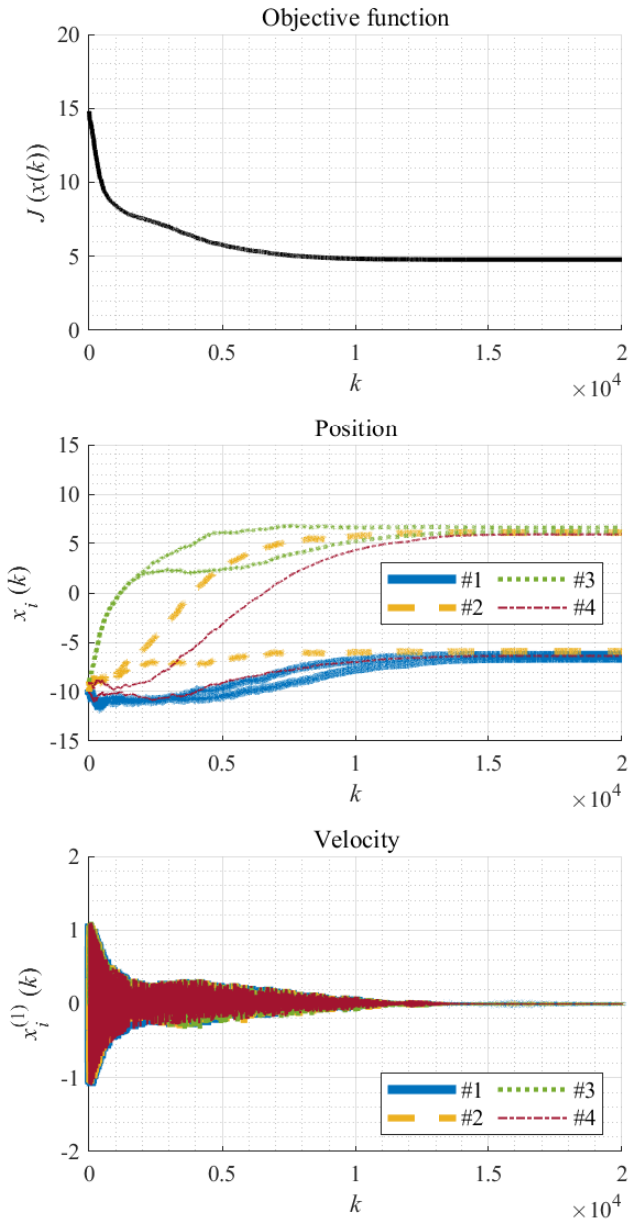

Figure 4.9: Time series of objective function (2.22), vehicles positions, and velocities by four-step local controller.

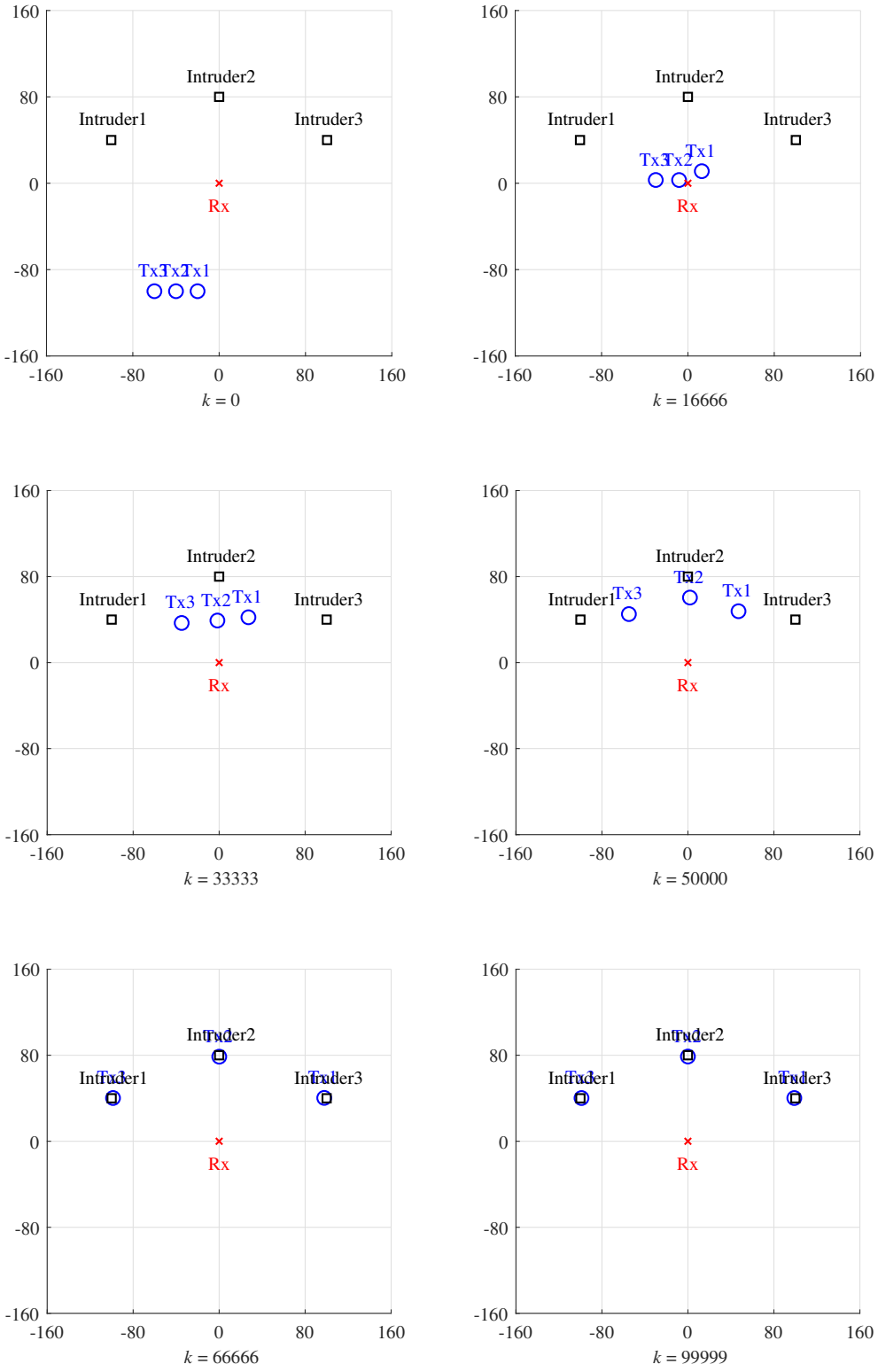

Figure 4.10: Snapshots of Tx, Rx, and intruders for case $\sigma(t) = 1$ and double-integrator system.

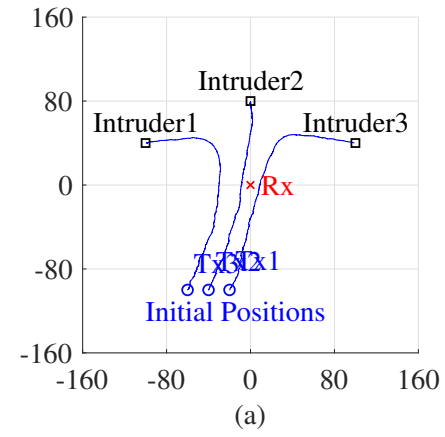

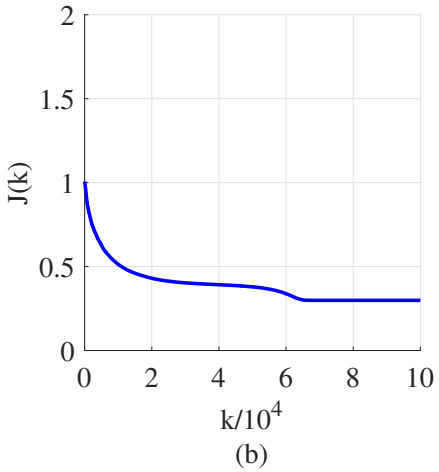

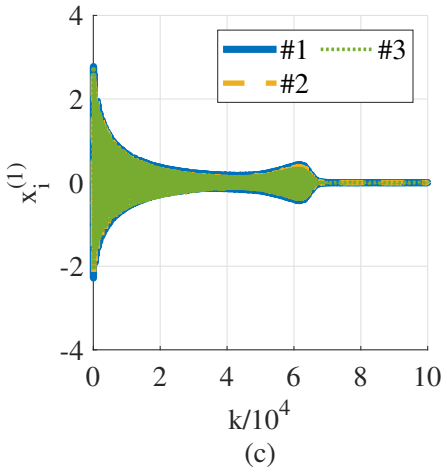

Figure 4.11: Trajectories of Tx and time evolution of $J(x(t))$ for case $\sigma(t) = 1$ and double-integrator system.

Chapter 5

Conclusion of Dissertation

This dissertation was concerned with the broadcast control, which is one of the new cooperative controls and is composed of the base station and multi-vehicle. Especially, we studied the new broadcast control for the anti-drone systems such as radar surveillance system and the case that the vehicle dynamics is the double-integrator system.

In the conventional radar surveillance system, the sensors for drone detection were mounted on the ground or the buildings. This seems to cause the target loss due to the weakness of the signal level and/or occlusion. Thus, we assumed the system composed of the base station with the receiving antenna and multi-vehicle with the transmission antenna, which meant that the sensors could move and the system had the capability of making the formation for drone detection. However, the radio wave propagation model was unknown due to the radar cross section of the drone and it was difficult to develop the cooperative control for the anti-drone system. On the other hand, the broadcast control did not need information about the system model and we focused on the control. In the conventional one, however, it was assumed that the base station measured the degree of achievement about the vehicles' positions and the vehicle dynamics was the single-integrator system. Then, we proposed two algorithms for the broadcast control as follows:

1. An algorithm for maximizing the degree of achievement about not the positions but the received signal level at the base station; we assumed that the vehicles had the transmission antenna and the reflected signals from the illegal drones were received at the base station.

2. An algorithm for the case that the vehicle dynamics is the double-integrator system.

In the future, we will also consider the other vehicle dynamics like the two-wheel vehicle system with the wheel-base parameter. Finally, we will evaluate the effectiveness of the experience using the actual vehicles and the base station.

Acknowledgement

First, I am grateful to Associate Professor Ryosuke Morita of Gifu University, Professor Tatsuya Suzuki of Nagoya University, and Professor Tsuyoshi Inoue of Nagoya University for many thoughtful comments on the research.

I would like to thank Associate Professor Toru Asai of Nagoya University for suggesting useful advice through my research.

I am grateful to Professor Shun-ichi Azuma of Kyoto University for the various discussions and pieces of advice in the research.

I also thank Associate Professor Ryo Ariizumi of Tokyo University of Agriculture and Technology for his helpful comments on my submitted papers.

Finally, I appreciate the continuous encouragement from my family.

Bibliography

[1] https://www.icao.int/Meetings/UAS/Documents/Circular%20328_en.pdf.

[2] https://www.dedrone.com/resources/incidents-new/all.

[3] https://www.icao.int/safety/UA/Documents/EASA%20Drone%20Incident%20Management%20at%20Aerodromes%20-%20Part%20I.pdf.

[4] https://www.bbc.com/news/uk-england-sussex-65591023.

[5] Xiufang Shi, Chaoqun Yang, Weige Xie, Chao Liang, Zhiguo Shi, and Jiming Chen. Anti-drone system with multiple surveillance technologies: Architecture, implementation, and challenges. *IEEE Communications Magazine*, 56(4):68–74, 2018.

[6] Seongjoon Park, Hyeong Tae Kim, Sangmin Lee, Hyeontae Joo, and Hwangnam Kim. Survey on anti-drone systems: Components, designs, and challenges. *IEEE Access*, 9:42635–42659, 2021.

[7] Muhammad Saqib, Sultan Daud Khan, Nabin Sharma, and Michael Blumenstein. A study on detecting drones using deep convolutional neural networks. In *14th IEEE International Conference on Advanced Video and Signal Based Surveillance*, 2017.

[8] Jihun Park, Dae Hoe Kim, Young Sook Shin, and Sang-ho Lee. A comparison of convolutional object detectors for real-time drone tracking using a PTZ camera. In *17th International Conference on Control, Automation and Systems*, 2017.

[9] Mouhyemen Khan, Karel Heurtefeux, Amr Mohamed, Khaled A. Harras, and Mohammad Hassan Mehedi. Mobile target coverage and tracking on drone-be-gone UAV cyber-physical testbed. *IEEE Systems Journal*, 12(4):3485–3496, 2017.

[10] Hyun Min Oh, Hyunki Lee, and Min Young Kim. Comparing convolutional neural network (CNN) models for machine learning-based drone and bird classification of anti-drone system. In *19th International Conference on Control, Automation and Systems (ICCAS 2019)*, 2019.

[11] Lianghui Ding, Xin Xu, Yuan Cao, Guangtao Zhai, Feng Yang, and Liang Qian. Detection and tracking of infrared small target by jointly using SSD and pipeline filter. *Digital Signal Processing*, 110:1–9, 2021.

[12] Jie Zhao, Jingshu Zhang, Dongdong Li, and Dong Wang. Vision-based anti-UAV detection and tracking. *IEEE Transactions on Intelligent Transportation Systems*, 23(12):25323–25334, 2022.

[13] Fatemeh Mahdavi and Roozbeh Rajabi. Drone detection using convolutional neural networks. In *6th Iranian Conference on Signal Processing and Intelligent Systems*, 2020.

[14] Chunanyun Wang, Zhongrui Shi, Linlin Meng, Jingjing Wang, Tian Wang, and Qian Gao. Anti-occlusion UAV tracking algorithm with a low-altitude complex background by integrating attention mechanism. *Drones*, 6(6):1–14, 2022.

[15] Xianyu Chang, Chaoqun Yang, Junfeng Wu, Xiufang Shi, and Zhiguo Shi. A surveillance system for drone localization and tracking using acoustic arrays. In *IEEE 10th Sensor Array and Multichannel Signal Processing Workshop*, 2018.

[16] Shulin Li, HyunJong Kim, Sukhoon Lee, John C. Gallagher, and Daeun Kim. Convolutional neural networks for analyzing unmanned aerial vehicles sound. In *18th International Conference on Control, Automation and Systems*, 2018.

[17] Zahoor Uddin, Muhammad Altaf, Muhammad Bilal, Lewis Nkenyereye, and Ali Kashif Bashir. Amateur drones detection: A machine learning approach utilizing the acoustic signals in the presence of strong interference. *Computer Communications*, 154:236–245, 2020.

[18] Ilhan Aydin and Emrullah Kizilay. Development of a new light-weight convolutional neural network for acoustic-based amateur drone detection. *Applied Acoustics*, 193:108773–108784, 2022.

[19] Erhan Akbal, Ayhan Akbal, Sengul Dogan, and Turker Tuncer. An automated accurate sound-based amateur drone detection method based on skinny pattern. *Digital Signal Processing*, 136:1–12, 2023.

[20] Farshad Koohifar, Ismail Guvenc, and Mihail L. Sichitiu. Autonomous tracking of intermittent RF source using a UAV swarm. *IEEE Access*, 6:15884–15897, 2018.

[21] Mohammad Al-Sa'd, Abdulla Al-Ali, Amr Mohamed, Tamer Khattab, and Aiman Erbad. RF-based drone detection and identification using deep learning approaches: An initiative towards a large open source drone database. *Future Generation Computer Systems*, 100:86–97, 2019.

[22] Nida Kumbasar, Rabiye Kilic, Emin Argun Oral, and Ibrahim Yucel Ozbek. Comparison of spectrogram, persistence spectrum and percentile spectrum based image representation performances in drone detection and classification using novel HMFFNet: Hybrid model with feature fusion network. *Expert Systems with Applications*, 206:1–13, 2022.

[23] Rabiye Kilic, Nida Kumbasar, Emin Argun Oral, and Ibrahim Yucel Ozbek. Drone classification using RF signal based spectral features. *Engineering Science and Technology, an International Journal*, 28:101028–101037, 2022.

[24] Boban Sazdic-Jotic, Ivan Pokrajac, Jovan Bajcetic, Boban Bondzulic, and Danilo Obradovic. Single and multiple drones detection and identification using RF based deep learning algorithm. *Expert Systems with Applications*, 187:1–15, 2022.

[25] Kamel K. Mohammed, Eman I.Abd El-Latif, Noha Emad El-Sayad, Ashraf Darwish, and Aboul Ella Hassanien. Radio frequency fingerprint-based drone identification and classification using Mel spectrograms and pre-trained YAMNet neural. *Internet of Things*, 23:1–15, 2023.

[26] Thomas Multerer, Alexander Ganis, Ulrich Prechtel, Enric Miralles, Askold Meusling, Jan Mietzner, Martin Vossiek, Mirko Loghi, and Volker Ziegler. Low-cost jamming system against small drones using a 3D MIMO radar based tracking. In *2017 European Radar Conference*, 2017.

[27] Jedrzej Drozdowicz, Maciej Wielgo, Piotr Samczynski, Krzysztof Kulpa, Jaroslaw Krzonkalla, Maj Mordzonek, Marcin Bryl, and Zbigniew Jakielaszek. 35 GHz FMCW drone detection system. In *17th International Radar Symposium*, 2016.

[28] Sirish Deshmukh and Vaibhav Sharma. An SDR-based anti-drone system with detection, tracking, jamming, and spoofing capabilities. In *IEEE Microwaves, Antennas, and Propagation Conference*, 2022.

[29] Ann Janeth Garcia, Ali Aouto, Jae-Min Lee, and Dong-Seong Kim. CNN-32DC: An improved radar-based drone recognition system based on convolutional neural network. *ICT Express*, 8:606–610, 2022.

[30] G. Fang, J. Yi, X. Wan, Y. Liu, and H. Ke. Experimental research of multistatic passive radar with a single antenna for drone detection. *IEEE Access*, 6:33542–33551, 2018.

[31] Y. Dan, J. Yi, X. Wan, Y. Rao, and B. Wang. LTE-based passive radar for drone detection and its experimental results. In *IET International Radar Conference (IRC 2018)*, 2018.

[32] R. S. A. R. Abdullah, S. A. Musa, Rashid N. E. A., A. Sali, A. A. Salah, and A. Ismail. Passive forward-scattering radar using digital video broadcasting satellite signal for drone detection. *Remote Sensing*, 12(18):1–26, 2020.

[33] D Poullin. UAV detection and localization using passive DVB-T radar MFN and SFN. *STO-MP-SET-231*, pages 1–10, 2016.

[34] `https://www.dedrone.com/products/counter-drone-software`.

[35] `https://www.robinradar.com/elvira-radar-integrated-in-guardion-modular-drone-defence-system`.

[36] `https://www.global.toshiba/ww/products-solutions/defense/c-uas/knowledge/counter-drone.html#counter-drone02`.

[37] `https://www.zentechnologies.com/anti-drone-system-counter-drone-cuas.php`.

[38] `https://www.homelandsecurity-technology.com/projects/anti-uav-defence-system-auds/`.

[39] `https://d-fendsolutions.com/ja/`.

[40] `https://www.adanidefence.com/counter-drone-systems`.

[41] `https://www.rafael.co.il/worlds/air-missile-defense/c-uas-counter-unmanned-aircraft-systems/`.

[42] `https://www.indracompany.com/en/anti-drone-system`.

[43] Xianxu Zhai, Zhihua Huang, Tao Li, Hanzheng Liu, and Siyuan Wang. YOLO-drone: An optimized YOLOv8 network for tiny UAV object detection. *Electronics*, 12(17):1–21, 2023.

[44] Jeff S. Shamma. *Cooperative Control of Distributed Multi-Agent Systems*. Wiley, 2007.

[45] Yasuhiro Kuriki and Toru Namerikawa. Control for formation configuration using leader and follower structure. In *The 55th Japan Joint Automatic Control Conference*, 2012.

[46] Takumi Matsuda, Toshihiro Maki, and Takashi Sakamaki. Accurate and efficient seafloor observations with multiple autonomous underwater vehicles: Theory and experiments in a hydrothermal vent field. *IEEE Robotics and Automation Letters*, 4(3):2333–2339, 2019.

[47] Takumi Matsuda, Toshihiro Maki, and Takashi Sakamaki. Navigation method of multiple AUVs with velocity control for stable positioning and communication among AUVs. In *OCEANS 2019*, 2019.

[48] Liangming Chen, Hector Garcia de Marina, and Ming Cao. Maneuvering formations of mobile agents using designed mismatched angles. *IEEE Transactions on Automatic Control*, 67(4):1655–1668, 2022.

[49] Takanori Komatsu, Tomoyuki Ohkubo, Kazuyuki Kobayashi, Kajiro Watanabe, and Yosuke Kurihara. A study of RSSI-based formation control algorithm for multiple mobile robots. In *SICE Annual Conference 2010*, 2010.

[50] Isa Ravanshadi, Elham Amini Boroujeni, and Mahdi Pourgholi. Centralized and distributed model predictive control for consensus of non-linear multi-agent systems with time-varying obstacle avoidance. *ISA Transactions*, 133:75–90, 2023.

[51] Vasilii Semkin, Mingsheng Yin, Yaqi Hu, Marco Mezzavilla, and Sundeep Rangan. Drone detection and classification based on radar cross section signatures. In *ISAP2020*, 2020.

[52] Vasilii Semkin, Jaakko Haarla, Thomas Pairon, Christopher Slezak, Sundeep Rangan, Ville Viikari, and Claude Oestges. Analyzing radar cross section signatures of diverse drone models at mmWave frequencies. *IEEE Access*, 8:48958–48969, 2020.

[53] Rui Fu, Mohammed Abdulhakim Al-Absi, Ki-Hwan Kim, Young-Sil Lee, Ahmed Abdulhakim Al-Absi, and Hoon-Jae Lee. Deep learning-based drone classification using radar cross section signatures at mmWave frequencies. *IEEE Access*, 9:161431–161444, 2021.

[54] Yasuo Fujishima and Shun-ichi Azuma. Broadcast control of radar surveillance systems for unexpected drones. *Asian Journal of Control*, 25(2):758–768, 2023.

[55] Shunichi Azuma, Ryota Yoshimura, and Toshiharu Sugie. Broadcast control of multi-agent systems. In *50th IEEE Conference on Decision and Control*, 2011.

[56] Shunichi Azuma, Ryota Yoshimura, and Toshiharu Sugie. Broadcast control of multi-agent systems. *Automatica*, 49(8):2307–2316, 2013.

[57] Yasuo Fujishima and Shun-ichi Azuma. Broadcast control of multi-agent systems with double-integrator vehicles (in Japanese). *Transactions of the Institute of Systems, Control and Information Engineers*, 2023.

[58] Shun-ichi Azuma. Multi-agent control : V coverage control. *Systems, control and information*, 58(1):36–44, 2014.

[59] J. Capon. High-resolution frequency-wavenumber spectrum analysis. *Proceedings of the IEEE*, 57:1408–1418, 1969.

[60] E. J. Naglak, C. Kase, M. McGinty, C. D. Majhor, S. C. Greene, P. J. Bos, and W. W. Weaver. Cable deployment system for unmanned ground vehicle (UGV) mobile microgrids. *HadwareX*, 10:1–12, 2021.

[61] Takashi Yoshida. *Radar engineering revised edition (in Japanese)*. IEICE, 2011.

[62] K. M. Siegel, H. A. Alperin, R. R. Bonkowski, J. W. Crispin, A. L. Maffett, C. E. Schensted, and I. V. Schensted. Bistatic radar cross sections of surfaces of revolution. *Journal of Applied Physics*, 26(3):297–305, 1995.

[63] Yongcan Cao, Daniel Stuart, Wei Ren, and Ziyang Meng. Distributed containment control for multiple autonomous vehicles with double-integrator dynamics:

Algorithms and experiments. *IEEE Transactions on Control Systems Technology*, 19.

[64] Yutao Tang and Peng Yi. Nash equilibrium seeking for high-order multiagent systems with unknown dynamics. *IEEE Transactions on Control of Network Systems*, 10.

[65] S. Boyd and L. Vandenberghe. *Convex Optimization*. Cambridge University Press, 2009.

Appendix A

Properties About Convexity and Concavity

We show the properties of convexity and concavity in the following lemma.

Lemma A.1. Convexity and concavity have the following properties [65].

(C1) Nonnegative weighted sums operation preserves convexity and concavity, that is, if the functions w_i $(i = 1, 2, \ldots, N)$ are convex (or concave),

$$w = \alpha_1 w_1 + \alpha_2 w_2 + \cdots \alpha_M w_N \tag{A.1}$$

is also convex (or concave) for the nonnegative coefficients α_i $(i = 1, 2, \ldots, N)$.

(C2) If the function w is concave and positive, then $\log w(k)$ is concave.